ACOUSTIC METHODS FOR REGIONALIZING AN IMPACT FORCE ACTING ON A HELMET STRUCTURE

by

JACOB ANDREW DAVIS

W. STEVE SHEPARD, COMMITTEE CHAIR
KEITH A. WILLIAMS
JAMES P. HUBNER

A THESIS

Submitted in partial fulfillment of the requirements
for the degree of Master of Science
in the department of Mechanical Engineering
in the Graduate School of
The University of Alabama

TUSCALOOSA, ALABAMA

2018

ABSTRACT

It is often desired to know the location and magnitude of a force acting on a structure. Unfortunately, it is not always possible or desirable to install a sensor at the force location, such as when the force location is unknown or when the application of a force sensor would change the force transmission characteristics. A structure subjected to an impact has many different vibrational modes that are excited to different levels based on the excitation location. These vibrations decay with time depending on their different rates of modal damping and the associated acoustic radiation characteristics. This response of the structure can be measured and used to inversely reconstruct the input force. It is theoretically possible to use acoustic measurements for force reconstruction, but the method involved would be extremely difficult. In this study, approaches that are much simpler and easier to implement were considered. Acoustic signatures for several structure impact locations were measured, normalized relative to the force magnitude, and processed to examine the ability to correlate the acoustic signal to the force impact location. Various processing techniques, such as the Short Time Fourier Transform, were considered. A primary interest focused on the ability of using single-number metrics that describe features of the acoustic signature to aid in identifying the force location. For the experiments, a football helmet structure was used and multiple impact locations on the helmet were tested. The ability of these acoustic signatures, including those processed into single-number metrics, to aid in identifying the impact location was assessed.

DEDICATION

For my family and friends, who kept me sane enough to see this through to the end.

LIST OF ABBREVIATIONS AND SYMBOLS

AK	Absolute Kurtosis
DTFT	Discrete Time Fourier Transform
c	Speed of Sound in Air (m/s)
∇	Vector Differential Operator
f	Frequency (Hz)
F	Force (lb_f)
FFT	Fast Fourier Transform
i	Imaginary Number
L	Length (m)
P	Pressure (Pa)
$\bar{P}$	Average Pressure (Pa)
P_{rms}	Root-Mean-Square Pressure (Pa)
$\emptyset_n$	Mode Shape
STFT	Short-Time Fourier Transform
t	Time (s)
ω	Angular Frequency (rad/s)
ω_n	Angular nth-modal Frequency (rad/s)
x	Position (m)
y	Transverse Displacement (m)
Y_n	Modal Response Amplitude (m)

ACKNOWLEDGMENTS

I would like to thank Dr. Keith Williams and Dr. Paul Hubner for being a part of my Masters Thesis Committee, their insight and support, and for their help in preparing this document. I would especially like to thank Dr. W. Steve Shepard for his assistance with my research and for being the head of my Thesis committee, as well as for his invaluable advice as I transitioned into Graduate School. I would also like to thank The University of Alabama and the professors and staff in the Department of Mechanical Engineering for all that I have learned over the last five years. Finally, I would like to recognize the STAL laboratory for the use of its equipment, as well as James Wiggins for his assistance in conducting the experiments. The research presented within would not have been possible without the support of all those listed above, nor without the support of my friends and family who never ceased to encourage me to keep going.

CONTENTS

LIST OF FIGURES

CHAPTER 1

INTRODUCTION

It is often desired to know the location and magnitude of an impact force acting on a structure, such as for a bird strike on an airplane. While measuring the vibrational response of a structure to an impact force is straightforward, having a measure of the input forces to a system can greatly help in the analysis of that system. Knowing the input forces is also helpful when characterizing real structures to diagnose problems either with the structure itself or the contents inside the structure. In recent years, this type of knowledge of input forces has become extremely valuable.

In the case of a planned excitation of a structure with a force, such as a manufacturing plant where machines often exert loads on each other, the location of the force input is usually known. Force magnitude measurements are read by force sensors placed at those force locations. However, in both planned and unplanned excitations, it is not always possible to place a sensor at the force location either due to geometric constraints or due to not knowing the impact location. In the case of large structures, placing sensors at many different locations can be impractical when the impact location is not known *a priori*. Additionally, the placement of sensors on the structure can change the system properties where the sensor is mounted, which can result in an inaccurate measurement of the force. Even though this change may be small, the change in mass from the addition of the sensor and the additional stiffness or damping that results from the attachment of the sensor can affect the impedance of the structure, which will change the

measured force. A better method for measurement in these cases is one that does not require force sensors mounted on the structure.

It is possible to reconstruct the input forces to a system using the response of the system (Craun 1999; Fubunmi 1986). This technique of using response measurements of the structure to determine the input forces to that structure is referred to as an inverse method. This method reconstructs the time history of the force magnitude, based on the measured response of the structure and an analytical system model. An acceleration sensor or another type of motion sensor records the response of the structure and the inverse system model is used to rebuild the force values. Note that these inverse methods are also able to reconstruct the location of a force when that location is initially unknown.

One area where force reconstruction is beneficial is in the medical field with the rise of research into concussions. Between 2005 and 2010, Jonathan Beckwith, research director at Simbex, conducted a study involving eight football teams to research helmet design and concussions (Beckwith 2012). His team placed accelerometer sensors inside the helmets of 1208 football players to measure the net acceleration of the players' heads during collisions. The accelerometer readings were correlated with diagnosed concussions and, using a simple inverse method, the overall force of the impacts was determined. However, this study only looked at the magnitude of forces and not ways to characterize the location of impact.

Reconstructing both the force location or magnitude using an inverse method presents many difficulties. Many inverse methods have been developed using vibration measurements. Most techniques involve the inversion of a frequency response matrix, which proves to be difficult and sometimes impossible. However, these methods have shown great ability to characterize both force locations and magnitudes. Even so, it is not always practical to install

vibration sensors on a structure. Very light structures cannot have vibration sensors mounted on them, and moving structures require wireless devices which are significantly more expensive.

It is possible to measure the response of a structure using a method that does not require any contact with the structure in question. Two possible methods for this type of hands-off measurement are laser doppler vibrometry (LDV) (Buckberry 1999) and acoustic measurements. From a practical perspective, LDV will not work on a moving structure as one can only scan in one dimension. Scanning laser vibrometer systems that measure motion in three dimensions are highly expensive, making using them for these measurements cost-prohibitive – particularly if the structure is moving.

The other possible solution for a non-contact measurement method is acoustic measurement. An impact on a structure will excite many different vibrational modes to different levels. These vibrational modes decay with time depending on the modal damping characteristics of the structure and the associated acoustic radiation characteristics. These vibration modes produce an acoustic response in the air around the structure which can be easily measured with one or more microphones.

Of course, there are drawbacks to using acoustic measurements for reconstructing the impact force and location. To date, there are no established practical approaches to applying acoustic measurements in an inverse force reconstruction method except for those techniques which utilize acoustic holography. Acoustic holography uses an array of microphones spread out across the field to comprehensively capture the acoustic signature at many points (Greussing 2012). Also, using acoustic measurements for force reconstruction is quite complex as both the model of the structure and a model of the acoustic environment around the structure would be

needed in order to accurately determine the force. An accurate model of the acoustic environment would be difficult to create.

Therefore, this thesis examines the feasibility of using acoustic readings to correlate with force characteristics. In this study, the hypothesis is that it is possible to remotely determine the impact location of a force acting on a structure using acoustic measurements and post-processing methods. To test this hypothesis, a football helmet is impacted at various locations across its surface and various signal processing techniques are applied in an attempt identify unique changes to the measured sound with impact location. Because of the very simplified approach, it is not expected that other features, like impact duration, can necessarily be inferred from the acoustic measurement. The goal is to examine the feasibility of identifying impact location using only the remotely-measured acoustic signature.

To measure an acoustic signature and perform a correlation study, it is important to run such tests in an environment that minimizes the reflection of sound waves. To that end, an anechoic chamber is used here. The anechoic chamber at the University of Alabama is shown in Figure 1.1. The foam tiles on the walls absorb the sound to prevent reflected waves so that the measurement at the microphone location is the original signal radiated only from the structure.

Figure 1.1 UA Anechoic Chamber.

In this study, impact locations are pre-selected on a football helmet and a force imparted at these locations with an instrumented impulse hammer. A diagram of the set-up is shown in Figure 1.2. The resulting acoustic response is measured at two microphone locations, one on each side of the helmet. Then, several different signal-processing methods are considered to help identify differences to the acoustic signature resulting from changes in the impact location. The methods considered in this research include the Short-Time Fourier Transform (STFT), Fast Fourier Transform (FFT), Kurtosis calculations in both time and frequency-domains, and root-mean square (RMS) analysis on the time-domain acoustic response. These analysis methods are used to examine a possible correlation between the acoustic response and the impact location on the helmet.

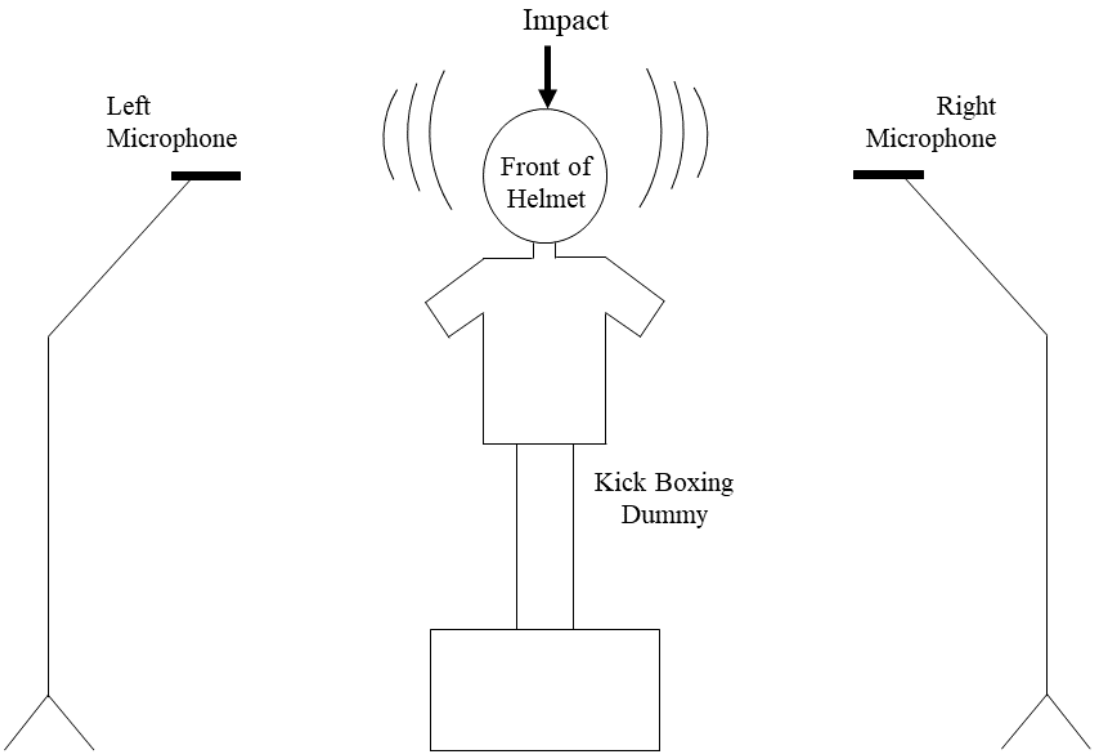

Figure 1.2. Diagram of experimental set-up.

The following chapter presents a review of relevant acoustic and vibrational theory, discusses literature surrounding inverse methods, and discusses the methodology behind the signal processing approaches used in this study. First, the fundamental equations of acoustic and vibration theory as they relate to acoustic measurements are reviewed. Then, the challenges of the inverse method are examined to provide a motivation for the simpler approach investigated. The next section provides a discussion of the operation behind the measurement devices used in this experiment. Finally, the considered signal processing approaches are described. Chapter 3 presents the experimental set-up used to acquire the acoustic readings and the method of taking these measurements. The fourth chapter discusses the experimental results and the results of applying the processing methods to the acoustic data. The final chapter presents the conclusions of this study as well as recommendations for future work.

CHAPTER 2

BACKGROUND AND LITERATURE REVIEW

This chapter presents an overview of some of the relevant theories and signal processing methods that relate to the research. This chapter is divided into three main sections that set the foundation for the work presented in this thesis. The first section presents a review of vibrational theory as it relates to the associated acoustic radiation, then a review of basic acoustic theory. The second section reviews the literature surrounding inverse methods and problems associated with these methods. Addressing some of the practical implementation problems provides the motivation for the work conducted here. The next section presents the operation of the equipment used in the experiments, and the final section highlights the mathematical approaches used in processing of the acoustic data obtained in the experiments.

2.1 Basic Vibration and Acoustic Theory

Although the structure considered in this research is a complex shaped polycarbonate helmet, it is possible to obtain some basic understanding of the helmet's response to an impulse by considering the response for a very simple structure, such as a string (Rao 2007). The response of a string fixed at both ends and plucked at a certain location, which responds similarly to a structure that receives an impulse, is given by

$$y(x,t) = \sum_{n=1}^{\infty} Y_n \emptyset_n \cos(\omega_n \mathrm{t} + \alpha_n) \ , \tag{1}$$

where ϕ_n is the mode shape for the string of length L given by

$$\emptyset_n(x) = \sin\left(\frac{n\pi x}{L}\right) . \quad (2)$$

The string has an infinite number of natural frequencies ω_n that will be excited to different levels Y_n when the string is plucked at a particular location. As the location of the excitation is changed, the mode shapes in the string which combine in different amounts dependent on the location where the string is plucked (Rao 2007). For a simple point impulse $\delta(x_o)$ at location x_o, the response Y_n of each vibration mode is given by

$$Y_n = \frac{2A}{\omega_n L}\sin\left(\frac{n\pi x_o}{L}\right). \quad (3)$$

where A is an amplitude that depends on the string properties. As can be seen in this equation, Y_n for each mode depends heavily on the force location x_o. As noted above, the structure considered here is much more complicated than a simple string. Nevertheless, the vibrational and thus associated acoustic response will depend heavily on the location of the impact force. This response dependence on the impact location is particularly true for a complicated structure like that considered in this research, namely a football helmet.

Any continuous structure, such as a football helmet, has an infinite number of natural frequencies that are excited to different levels when an impulse is imparted to the structure. The impulse delivered to the structure in this research is assumed to occur over a significantly short time period in the form of an impact force. The impulse acts like an initial velocity condition imposed on the structure, which will cause the natural frequencies to vibrate at their associated amplitudes (Tongue 2002). Of course, in the problem at hand, the interest is in the radiated acoustic pressure.

For a linear acoustic system, several assumptions apply; there is no mean velocity in the medium, the acoustic density and pressure are small relative to atmospheric quantities, the

particle velocity is very small relative to the speed of sound, and the medium is an ideal gas. Using these assumptions in the mass continuity equation, equation of state, and Newton's Second law, the acoustic pressure, *P*, is described by the linear acoustic wave equation (Kinsler 2000)

$$\nabla^2 P = \frac{1}{c^2}\frac{\partial^2 P}{\partial t^2} \quad . \tag{4}$$

The variable *c* in equation (4) represents the speed of sound in air, roughly 343 m/s or 1,128 ft/s at 20ºC or 70ºF. This equation represents a simple acoustic wave moving through homogeneous air with no variations in temperature across the medium. These factors both apply to acoustic testing inside an anechoic chamber since normal air can be approximated as homogenous, and the temperature is controlled. More details associated with the testing environment are given later.

One of the main problems in recording acoustic signatures due solely to a vibrating structure is the possible contamination of the data caused by reflections of pressure waves from nearby structures (Kinsler 2000). Rigid surfaces will reflect pressure waves back and distort the original acoustic signal unless they are damped well enough to negate their effect on the original acoustic signature. An anechoic chamber provides an acoustic field that is free of reflections through the placement of heavily absorbent acoustic foam in a pattern on the walls. As seen in Figure 2.1.1., this acoustic foam has a triangular shape in sets of three. This arrangement is rotated and repeated across the interior surface of the chamber. In addition to absorbing incident sound, the triangular arrangement redirects any remaining acoustic reflections into other nearby foam wedges by angling them further into the crevice of the foam until the energy has dissipated to a point where it is negligible in comparison to the original acoustic signal. While the chamber used in these experiments was configured in an anechoic configuration, there is a plastic floor

grating that may introduce reflections at high frequencies. As a result, a method used to deal with these possible issues by placing foam wedges along the floor is discussed in the next chapter.

Figure 2.1.1. Acoustic Foam

2.2 Inverse Method Overview

At this point, the basic vibration and acoustic theory discussed have assumed knowledge of the magnitude and location of the input forces. In many situations, these forces are not known beforehand and must be determined through experimental testing. Often, it is not possible to directly measure that input force for one or many reasons. For example, the application of a force sensor to the structure can change the transmission characteristics of the force, which results in a measurement that is not the same as if the sensor were not used (Avitabile 1999). It can also be the case that the physical geometry prevents the application of a force sensor, such as in confined environments or in structures where the added weight of a sensor is a factor.

These situations where a force sensor cannot be applied have necessitated the

development of force reconstruction methods. In these problems, the response of the structure is measured and used to inversely compute, or reconstruct, the applied force. Methods for reconstructing the force from the response are called inverse or reconstruction methods, since the force is a calculated quantity and not directly measured (Craun 1999; Fabunmi 1986; Liu 2005; Liu "An Improved Method" 2006; Liu "Reducing" 2006). These methods are often computationally expensive as they require the use of the inverse of the system model, which often involves a large matrix.

In a simple model of a forced multi-degree of freedom system, the vibration response of the structure can be represented by

$$\{x\} = [D]\{F\} \tag{5}$$

where the matrix [*D*] represents the system model and $\{F\}$ represents the input force vector (Rao 2007). Equation (4) can be manipulated to find $\{F\}$,

$$\{F\} = [D]^{-1}\{x\} \tag{6}$$

for cases where the response vector *{x}* is instead known, such as through a measurement. To reconstruct the input forces using this method, the inverse of matrix [*D*] must be found. This matrix can take many forms depending on the type of measurements used. If matrix [*D*] is not a square matrix, meaning there are more measured responses then forces to be computed, then the pseudoinverse must be used (Fubunmi 1986). Inverse methods can be difficult to implement because the inversion process is often ill-posed or ill-conditioned (Hansen 2001). When the inverse of a matrix is utilized small errors in the measured response can be magnified in the process of reconstructing the force. The inverse force reconstruction can also include large errors if the system model is near an instability (Thite 2006). If the system is ill-posed or ill-conditioned, finding the inverse of this matrix is often difficult and can sometimes be impossible.

As a result of these issues, implementing force reconstruction via a measured response can be computationally expensive. Of course, these methods also require sensors mounted directly onto the surface of the structure.

It is theoretically possible to use acoustic measurements for force reconstruction via the inverse method. This is even more difficult than using measurements of surface vibrations as the acoustic radiation needs to be included in the system model that is inverted in equation (6). This method would be quite complicated to implement even with knowledge of the structures radiation characteristics. To address this problem, but from a simpler perspective, the study conducted here looks at relating the impact force location to the measured acoustic signal. To infer information about the force location, various signal-processing techniques are considered in lieu of using a full inverse approach. This initial simplified approach involves using the Fast Fourier Transform, Short-Time Fourier Transform, and single-number metrics. These methods are used to hopefully infer basic information about the location of an impact force acting on the structure. One of the advantages of using acoustics is that sensors do not have to be mounted on the structure. As a result, the response can be measured remote to the structure. Because of the difficulty associated with a full acoustic inverse approach, this study is an initial investigation into such a method that starts with some simpler approaches.

To be able to use acoustic measurements to infer impact location, the existence of a relationship between an impact at known locations and the associated acoustic signature must be established. Then, the acoustic responses found through experimental methods can be studied via post-processing to help determine if it is feasible to use the processed acoustic signature in identifying the impact location. Conducting these experiments requires the use of several pieces of equipment discussed in the next section.

2.3 Equipment Operation

For the initial tests aimed at identifying a correlation between impact location and the processed acoustic signal, various instrumentation is used. To ensure some consistency in the force impact as well as for later processing, an impulse hammer is used to measure the force delivered during an impact to the structure. The hammer operates using a low impedance force sensor made of quartz along with an associated onboard amplifier that delivers a corresponding voltage to the data acquisition system. The hammer's onboard electronics need to be powered with an external power source, which can be from the data collection device. The hammer can normally be fitted with a variety of different tips of varying hardness as well as different masses for various applications. The different tip materials produce pulses of different duration when used to strike a structure. The plastic tip creates a longer pulse and the metal tip a shorter pulse which has a broader frequency spectrum for the excitation.

There are a variety of different sensing methods for microphones. The most common type used in acoustic research is the condenser microphone. This type of microphone has better sensitivity than a common dynamic microphone. The condenser microphone requires a power supply, which applies a voltage across the two plates of the capacitor inside the microphone sensing element. One of these plates acts as a diaphragm which moves in response to the acoustic pressure wave. The change in distance between the plates causes a change in the capacitance which causes current to flow (Peterson 1980).

The electric current produced by the condenser microphone is extremely weak, so a pre-amplifier is normally used for accurate measurement. This pre-amplifier is attached directly to the microphone and takes the weak signal from the microphone and amplifies it before sending it to the signal analyzer.

The other type of microphone used in this study is a piezoelectric microphone. This microphone uses a piezoelectric material, which generates a voltage in response to strain, attached to a diaphragm which bends the piezoelectric material in response to acoustic waves (Peterson 1980). The signal analyzer has the means to provide the necessary power for the amplifier built within this microphone as well.

A signal analyzer is a data collection device that processes electrical signals and converts them into engineering units, and can also perform other processing functions such as applying an anti-alias filter, windowing, and the Fast Fourier Transform (Peterson 1980). An impact hammer has a characteristic force sensitivity, and a microphone has an associated pressure sensitivity. These sensitivities are numerical conversion factors for converting the electrical signal sent from either device into an engineering unit. These sensitivities are programmed into the signal analyzer which then does the conversion instantaneously.

The signal analyzer records the reading from one or more devices in time, and can also process these signals by a Fourier transform method. Normally the method used is the Fast Fourier Transform, where the results can then be viewed on a linear scale or logarithmic scale, also known as a decibel (dB) scale. The Fast Fourier Transform and other mathematical approaches are discussed in more detail in the next section. Because the goal here is to examine the effectiveness of various signal processing approaches to enable one to differentiate between impact force locations, the signal processing will be done in post processing using MatLab®. As a result, the dynamic analyzer will simply be used for anti-aliasing and the capture of time-domain data in appropriate engineering units.

2.4 Mathematical Approaches

There are many useful signal processing methods available for examining a correlation

between the impact force location and the measured acoustic signal. One common method for analyzing vibration and acoustic signals is Fourier analysis. The Fourier Transform (FT) is useful for this frequency analysis. The related Fast Fourier Transform (FFT) is an algorithm for computing the Discrete Fourier Transform faster, and is useful for frequency spectrum analysis. The FFT method analyzes a signal consisting of discrete points and returns the frequency components of the entire sample (Brigham 1974). These signal processing methods, which are used to examine the time-domain data, are now described in more detail.

The Fourier Transform (FT) us a mathematical approach for decomposing time-domain functions into the associated frequency components of that function. In the most basic sense, the FT is simply a translation from the time-domain into the frequency-domain (Kreyszig 2011). The term Fourier Transform refers to the continuous transform, which is mathematically described by

$$P(f) = \int_{-\infty}^{\infty} P(t) e^{-2\pi i f t} dt \tag{7}$$

where *f* represents the frequency in Hertz, and *P* represents the pressure.

The Discrete Time Fourier Transform (DTFT) is a useful variation of the continuous Fourier Transform. The DTFT applies the FT to discrete points obtained from sampling a continuous function, such as a continuous pressure wave in an acoustic signal. That evenly spaced time-domain data set is assumed to constitute the fundamental period of an infinitely periodic function. The Short Time Fourier Transform (STFT) is a version of the DTFT that applies the DTFT to a subset of the time-domain data (Brigham 1974). The process identifies the frequencies present in just that window of data. The STFT can then be repeated for a number of time locations throughout the time domain. This allows the frequencies of the function to be examined as they vary with time. Figure 2.4.1 shows a graph that illustrates the process of obtaining the STFT.

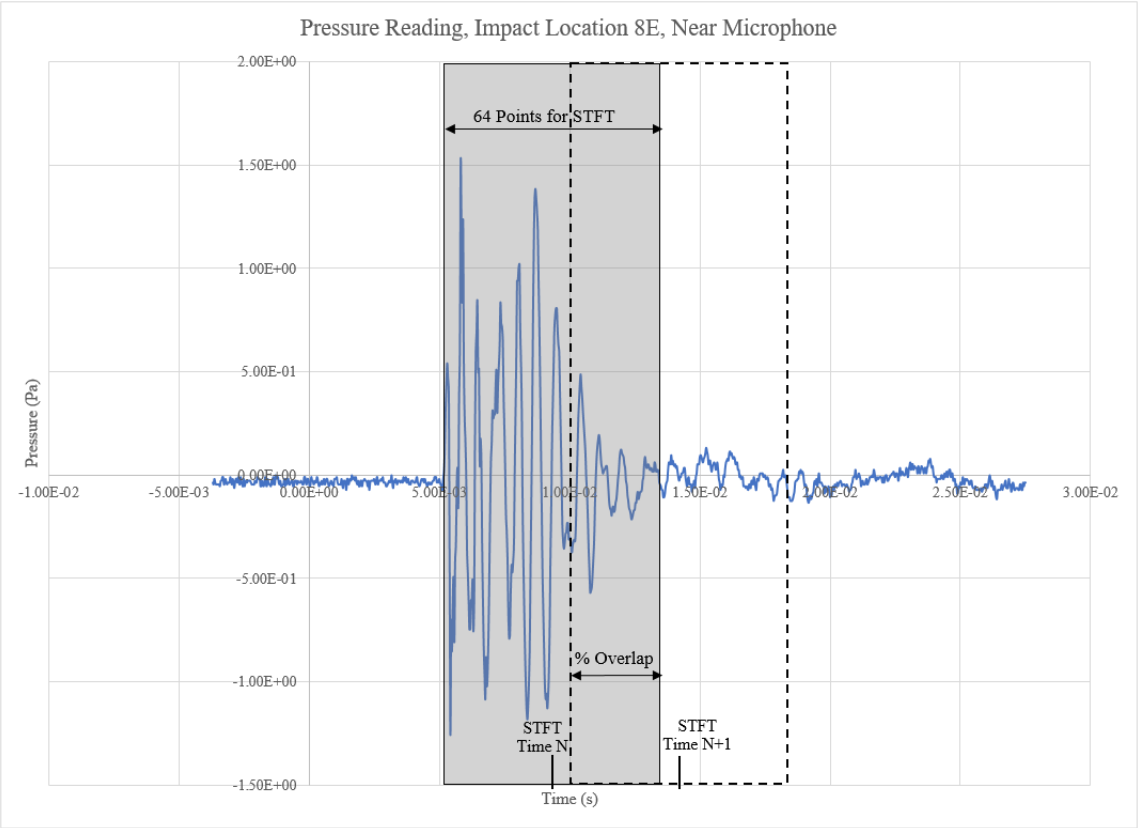

Figure 2.4.1. Sample Acoustic Signal detailing STFT Method (no scale, illustration only).

This figure shows an example acoustic signal that decays with time, which is a sample time signal from the structure considered in this research. The STFT is performed over a finite time period, which is specified by a number of points within the shaded region. In this study, a 64-point STFT was performed on a signal that has an overall length of 1024 points. While more points can be used in the STFT, there is a trade-off in the frequency versus time resolution. More points means better frequency resolution, but the time resolution decreases. The frequency amplitudes obtained for this first STFT are recorded as belonging to a specified time value at the center of the shown STFT window. Then, the time span is shifted down the time axis and the STFT is performed again at this new time value for the window center. The time shift is specified by a percentage of overlap between the first and second window time spans. A smaller

time window enables one to better identify when the frequencies occur in time. Unfortunately, there is a trade-off in frequency resolution as the window size is decreased. Therefore, the results will change as the window size is changed. For illustration purposes, the result of the STFT with a 90% overlap for the example acoustic signal above is shown in Figure 2.4.2. The results show that harmonic components in the range between 1,000 and 1,500 Hz occur about 7 ms into the data.

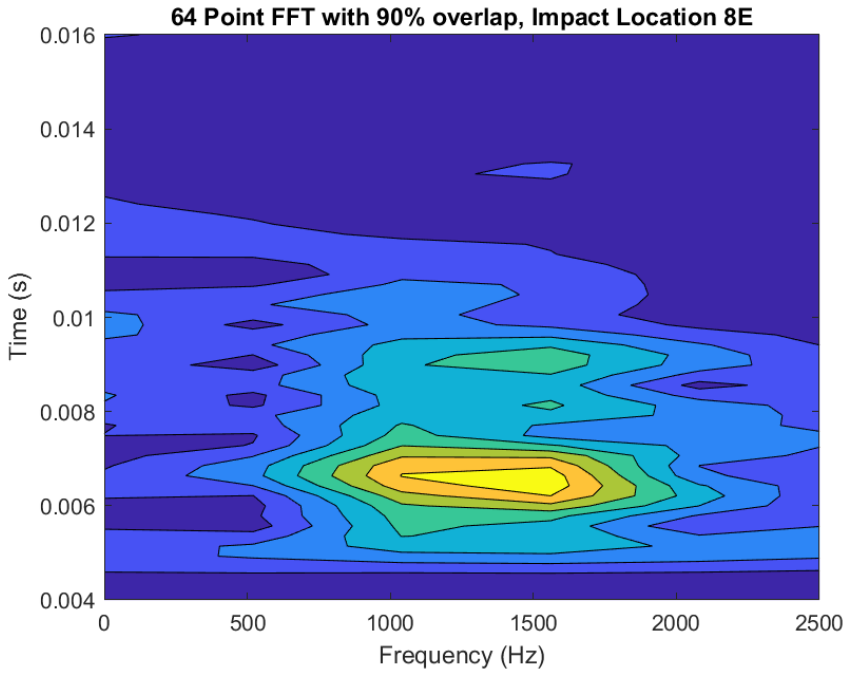

Figure 2.4.2. STFT Plot for Sample Acoustic Signal

Because this work is interested only in variations of pressure, the acoustic signals are zero-averaged to remove any DC offset in the measured pressure readings. To achieve this, a portion of the acoustic signal where it is known there is no sound associated with radiation from the structure is averaged to find the mean value. This mean value is then subtracted from the from the entire data set to remove that DC component.

Although the STFT can possibly provide insight regarding how the acoustic signal will

vary with impact location, it may not be an easy technique to implement for correlating a measured signal with an impact location. Therefore, other analysis techniques unrelated to the Fourier Transform are considered. These single-number metrics are values that characterize a certain aspect of the system acoustic response into a single value.

A simple single-number metric is the root-mean-square (RMS) of an oscillating signal. RMS is a method for finding the rectified average value of a sinusoidal function. Here, it will be applied to the time domain pressure signal as one approach for characterizing the acoustic response using a single-number metric. If *P(t)* represents the function in question, then the RMS value of the discretely sampled data is calculated as

$$P_{RMS} = \sqrt{\frac{\left[\sum_0^n \left(P(t_n)\right)^2\right]}{n}} \tag{8}$$

where *n* is the number of points in the sample. This function returns a single value which is the average magnitude of the rectified function. The RMS pressure can be calculated for the entire time-domain response or for only a subset of the time-domain response, depending on how one wishes to characterize the signal. Because this RMS-approach is a global measure of energy it is not initially expected to provide much insight on impact location. Nevertheless, it is one of the methods considered in the work.

Another single number metric investigated in this study is Kurtosis. The absolute Kurtosis is the fourth moment of a function about the average of the function (Kaltenbach 2012)

$$AK(P) = \frac{1}{I}\sum_{i=1}^{I}(P_i - \bar{P})^4 \quad , \tag{9}$$

where P_i is the pressure value and $\bar{P}$ is the average value of *x*. The Absolute Kurtosis of a signal is a metric that indicates major peaks within the signal. Relatively large peaks in a signal cause

larger values for Kurtosis. The Kurtosis is often applied in vibration monitoring (Keller) and has shown to be effective in some of those methods, thus providing a motivation for considering it here.

2.5 Concluding Remarks

This chapter presented an overview of basic acoustic theory, mathematical concepts and research related to force reconstruction. To date, all published applications of force reconstruction involve the use of inverse methods, which are difficult and computationally expensive to use, and require sensors mounted on the structure. There is a potential to use methods that utilize acoustic measurements, but those are even more complex, relatively speaking. As a result, methods that instead process the measured acoustic signal to simpler metrics are investigated in this study, to characterize basic information about input forces through remote measurements. The third section detailed the operation behind several devices that will be used in this experiment. The last section introduced mathematical analysis methods for examining acoustic signals. The following chapter provides a discussion of the set-up used to test for correlations between impact force location and acoustic radiation.

CHAPTER 3

EXPERIMENTAL METHOD OVERVIEW

This chapter discusses how the acoustic signals are measured inside the anechoic chamber for a given impact location on the test structure. While the previous chapter outlined the basic operation of the equipment, specific test methods and device settings are described here. In the first section, the different types of equipment used are explained as well as their importance. The second section discusses the experimental set-up as well as the different settings on the signal analyzer and why those settings were chosen. Section 3.2 explores the different types of tests performed to capture both force level and acoustic pressures to correlate the relationship between location and acoustic signature.

3.1 Experimental Equipment

Many different pieces of equipment were used to measure the acoustic signals in this experiment: a pair of microphones, a signal conditioning amplifier, and a signal analyzer. Prior to testing, a sound calibrator was used to verify the microphone setup and equipment settings. During testing, an impulse hammer was used to measure the force imparted to the structure. All testing was performed inside the anechoic chamber in the Alabama Institute for Manufacturing Excellence (AIME building) on campus. This equipment and testing process will now be described in more detail

The signal analyzer was a Hewlett-Packard 35670A Dynamic Signal Analyzer. This signal analyzer is capable of recording up to four signals at once over a frequency range of 25.6 kHz for each channel. Only three channels were used in this study, two for the microphones and one for the impact hammer. The analyzer is also able to provide power for the operation of amplifiers within piezoelectric device sensors. One of the primary features of this signal analyzer is that it can perform a real-time FFT to analyze the frequency spectrum of a signal, although that feature was not used in these tests. The analyzer has options for multiple types of windowing and can analyze a power spectrum based on the standard reference pressure for acoustics of 20 µPa. The signal analyzer is pictured in Figure 3.1.1. The labeled parts in Figure 3.1.1 include

1. the ICP power supply and input cable for the impulse hammer,
2. the ICP power supply and input cable for microphone type 4189,
3. the input cable for the microphone type 4191.

Figure 3.1.1. Hewlett-Packard 35670A Dynamic Signal Analyzer.

Both microphones used were made by Brüel & Kjær and operate as described in section 2.3. One of the microphones was a type 4189, which is a piezoelectric microphone with a pressure sensitivity of 53.2 mV/Pa; it is shown in Figure 3.1.2 (a). This microphone had a frequency range of 3.15-40000 Hz and was powered by the ICP power supply on the signal analyzer. The other microphone was a type 4191, which is a condenser microphone with a pressure sensitivity of 12.8 mV/Pa and had a frequency range of 6.3-20000 Hz; it is shown in Figure 3.1.2 (b). This type 4191 microphone required a special conditioning amplifier to provide the polarization voltage as described in section 2.3; this polarization voltage was 200 V.

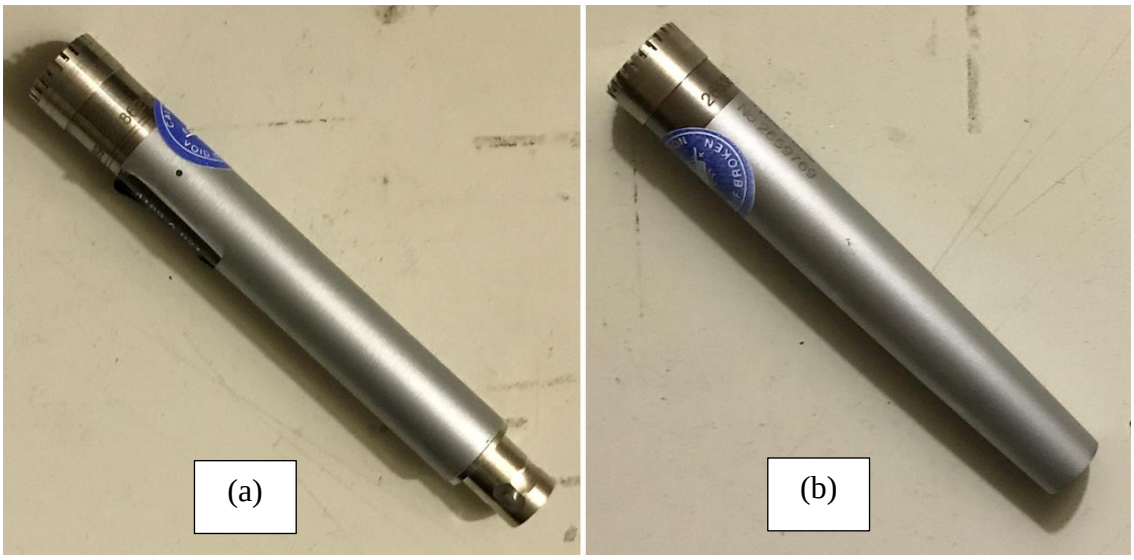

Figure 3.1.2. Brüel & Kjær microphone type 4189 (left) type 4191 (right).

The signal conditioning amplifier was also a Brüel & Kjær and is shown in Figure 3.1.3. The conditioning amplifier provides the pre-polarization voltage, receives the measured voltage output from the type 4191 microphone and displays the current user-selected sensitivity, which was 31.6 mV/Pa for these experiments.

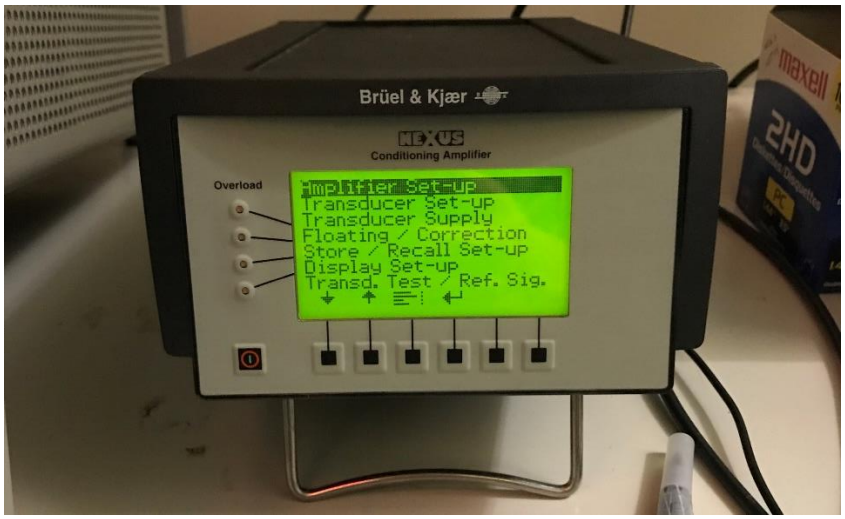

Figure 3.1.3. Brüel & Kjær Conditioning Amplifier.

The impact hammer used was a Kistler 9722A2000, which has a sensitivity of 10 mV/lb. This hammer also operates by a piezoelectric crystal as explained in chapter 2 and is powered by the ICP power supply built into the signal analyzer. The tip of the hammer used for striking the helmet is a metal tip. The hammer was equipped with an extender mass also made by Kistler, a type 9922. The mass of the extender was 50 grams. The hammer and extender mass are pictured in Figure 3.1.4.

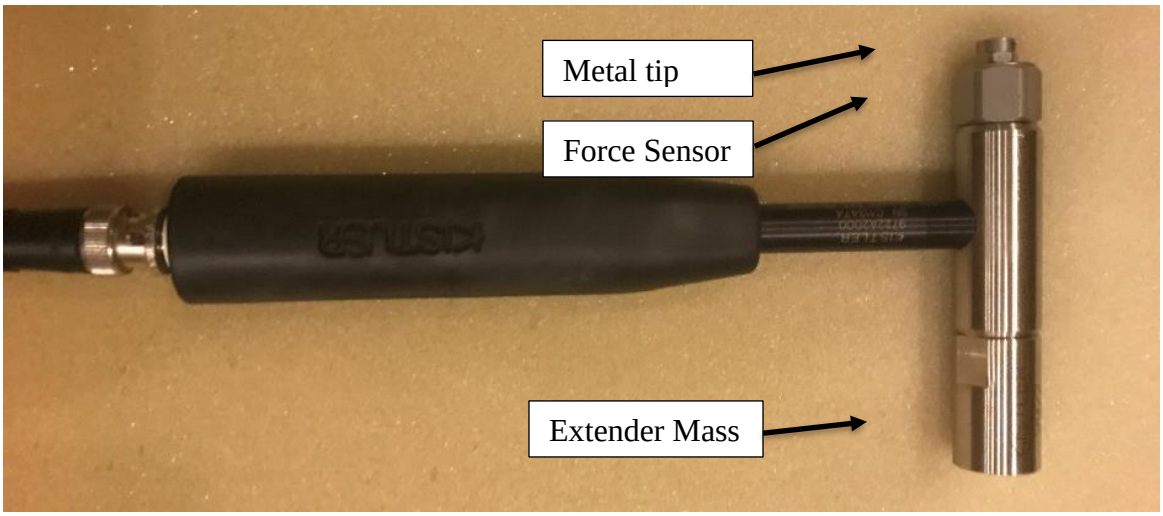

Figure 3.1.4. Kistler type 9722A2000 impulse hammer with 50-gram extender mass.

It was necessary to confirm that the microphone and signal analyzer settings were appropriate and that the devices were functioning properly before each round of testing. To this end, a sound calibrator was used to ensure proper microphone function. As seen in Figure 3.1.5, this sound calibrator is an electronic pistonphone that generates a pure tone of sound at 250 Hz and 124 dB. This pistonphone was placed over the microphone after the microphone was attached to the signal analyzer. The analyzer reads the frequency and dB level of the signal produced by the pistonphone. The sensitivity level of the microphones used in the analyzer to provide engineering units was verified with this sound calibrator. This was the only time the dB level was measured using the signal analyzer. All other recordings for the microphones are in Pascals (Pa) and in the time domain.

Figure 3.1.5. Sound Calibrator Type 1253.

Because it is desired to examine possible impact location identification methods for a complex structure, the structure chosen for this experiment is a football helmet made by Riddell. Although any structure could be used, as noted above, the motivation for using a helmet is that it is a fairly complicated structure that would be difficult to instrument for use in an inverse method. The helmet was a Riddell Youth Revo Edge Football Helmet made of polycarbonate and a steel facemask with foam padding on the inside. In this experiment, the helmet was mounted on top of a kickboxing dummy in order to simulate the effect of being on the head of an actual person. The boxing dummy used was a Body Opponent Bag made by Century. The helmet

is pictured in Figure 3.1.6, and the mounted setup in section 3.2. The helmet in Figure 3.1.6 is not the actual helmet tested, but is the same model. Furthermore, with a recent interest in football player concussions, there is an interest in developing force inverse methods for such structures. If one could use an acoustic method to remotely infer information about an impact caused by a helmet collision, there would be significant potential applications. Therefore, the helmet was chosen for these experiments.

Figure 3.1.6. Riddell Football Helmet.

3.2 Experimental Method

While the Riddell football helmet was mounted on the kickboxing dummy without the chinstrap, there was a fairly tight fit of the helmet on the dummy to prevent movement during testing. The chinstrap was left off due to interference with impact locations. The helmet and kick-boxing dummy were placed in the center of the anechoic chamber. This set-up can be seen in Figure 3.2.1.

Figure 3.2.1. Helmet and boxing dummy assembly in the UA anechoic test chamber.

On both sides of the helmet, the Brüel & Kjær microphones were placed six feet away from either side of the helmet surface. The type 4189 microphone was placed on the same side of the helmet that was to be impacted, on the left side of the helmet assembly as viewed from the front in Figure 3.2.2; this microphone will be referred to as the left microphone throughout the remainder of this thesis. The type 4191 microphone was placed on the right side of the helmet assembly as viewed from the front in Figure 3.2.2; this microphone will be referred to as the right microphone throughout the remainder of this thesis. The two microphone locations were used only to investigate the symmetry of the acoustic signature. Only the left microphone was used in the studies investigating changes associate with different impact locations.

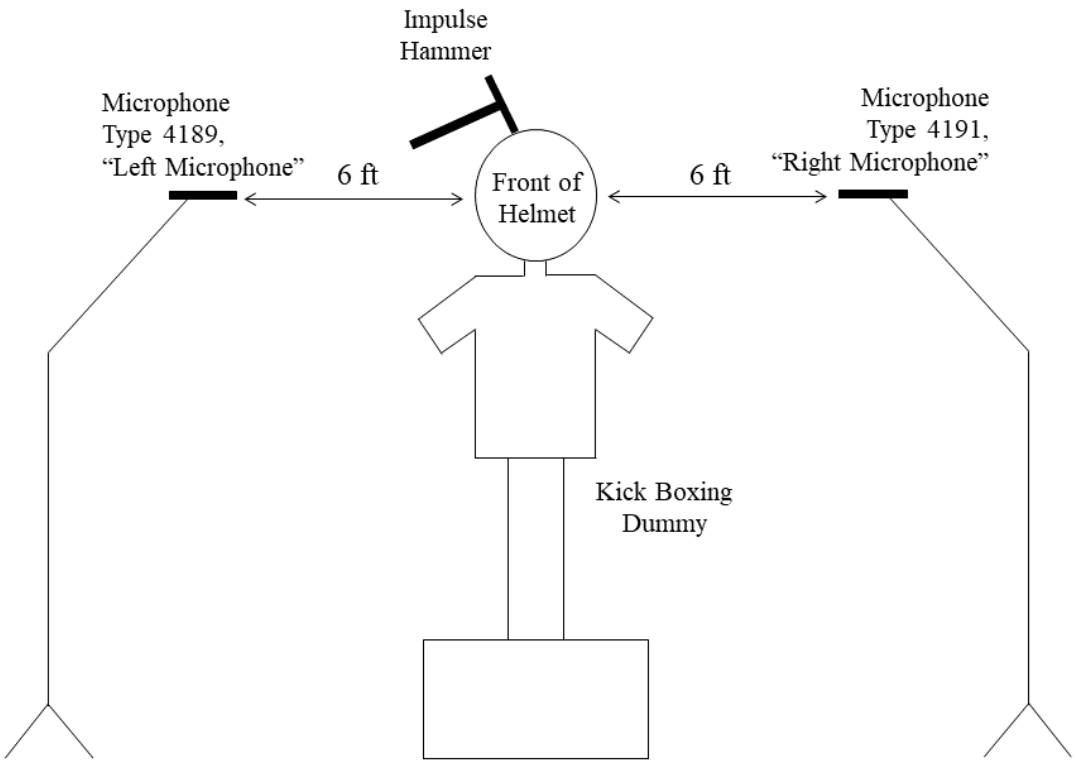

Figure 3.2.2. Experimental set-up inside the anechoic chamber.

Although this test was conducted inside an anechoic chamber, possible high-frequency reflections off the plastic floor grating were a potential concern. To prevent these high-frequency reflections, the floor surrounding the boxing dummy was covered in spare acoustic foam wedges. The low frequency sound was absorbed by these foam wedges as well as those located under the plastic floor grating and configured similarly to those on the wall panels in the chamber.

The microphones and impulse hammer were attached to the signal analyzer as shown back in Figure 3.1.1. The impulse hammer was connected to channel 1 and the type 4189 microphone to channel 2 on the signal analyzer. The type 4191 microphone was connected to the conditioning amplifier, and the conditioning amplifier was connected to channel 3 on the signal analyzer. The signal analyzer was configured to provide power to both the type 4189 microphone and the impulse hammer. The sensitives of all three devices were programmed into the signal

analyzer. A frequency span of 12.8 kHz was chosen for the analysis. This frequency span controlled the length of the recorded signal, which came out to be 31.22 ms, including the pre-trigger time (discussed below), and recorded 1024 data points for each channel. This time span was sufficient since the acoustic signals from the helmet impacts decay quickly, within less than 20 ms.

To control exactly when data is acquired, a trigger was set-up on the signal analyzer for the impulse hammer channel. Before each trial the signal analyzer was armed to await a trigger condition from the hammer output. A pre-trigger of 3.72 ms was used to ensure the whole signal from the impulse hammer and both microphones was captured, although the latter should be sufficiently delayed due to the speed of sound. This pre-trigger retains data in time prior to the moment the trigger condition is met, which occurs when the force reaches a prescribed level. Since all data processing was to be performed after collection, a rectangular window was set on the signal analyzer. This ensured there was essentially no windowing of the time-domain data for pressure and force and the data was reported as-is within the measured time window. It is worth noting that windowing is applied in the post processing in MatLab®, which will be described later.

To keep track of the impact locations across the hemisphere of the helmet, a grid was sketched directly onto the helmet surface. If the helmet is assumed to be uniform and symmetric, the acoustic signature for equivalent impact locations on either side of the helmet should simply swap microphone readings (e.g. left becomes right). This symmetry, if valid, results from the microphone and testing configuration. Therefore, to minimize the number of impact locations to be tested, the grid was only laid out on one hemisphere of the helmet and acoustic measurements taken on both sides. An unwrapped version of this grid is shown in Figure 3.2.2, and the

hemisphere of the helmet with the grid is shown in Figure 3.2.3. A larger version of the grid in Figure 3.2.2 is given in Appendix A. Note that not all points were used in the experiments conducted here. Some of the points within the finer grid resolution and not labelled will be reserved for later follow-up testing.

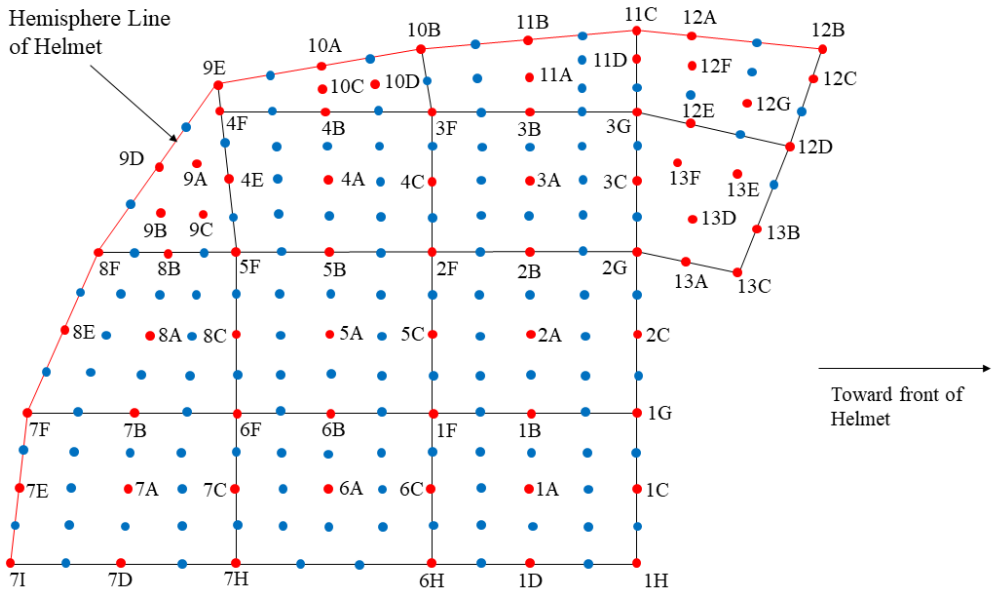

Figure 3.2.3. Helmet Grid map.

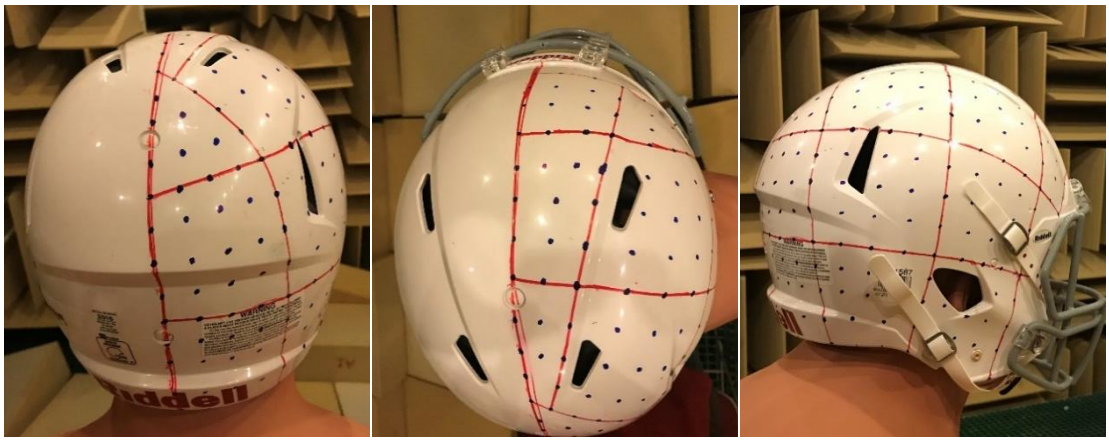

(a) Back of Helmet (b) Top of Helmet (c) Side of Helmet

Figure 3.2.4. Layout of Grid on Helmet.

The first round of tests involved investigating the relationship between the input force level and the acoustic response level of the helmet. This round was performed to determine whether there were any possible non-linearities within the tests. Three impact locations were chosen along the crown of the helmet: 8E, 10B, and 12B. At each impact location, three different levels of impulse were imparted: a soft impact, a medium impact, and a large impact.

The second round of tests involved measuring the acoustic response from an impact at each of 70 impact locations to examine the existence of a possible relationship between the impact location and the radiated acoustic signature. As noted above, there were more points laid out on the helmet than were impacted. The 70 impacted locations are shown as red dots in Figure 3.2.2 and are labelled. For all 70 points shown in the figure, the impact was recorded as well as the pressure readings from both microphones. In both rounds of testing, the experimenter stood either directly behind or directly in front of the helmet assembly. The signal analyzer and conditioning amplifier were both placed outside the anechoic chamber to reduce background noise. Background noise was not an issue as there was no moving machinery inside the anechoic chamber and the chamber was acoustically sealed for both rounds of testing. The acoustic data also indicated that background noise was not an issue.

For both rounds of testing, after each impact the time domain signal of the force and the time domain signal of the pressure readings were each recorded in a text file and transferred to a computer for post-processing. These data files were combined into a single Excel® file and later exported to Matlab® for signal processing. The next chapter will detail how the processing methods described in section 2.4 were applied to this data.

3.3 Concluding Remarks

This chapter provides a detailed overview of the experimental process used to record the acoustic response of the helmet to force impacts at various locations. Various equipment settings and test methods are also discussed. In the next chapter, a detailed discussion of the analysis performed on the data is given.

CHAPTER 4

EXPERIMENTAL RESULTS AND DISCUSSION

This chapter presents the results of the tests performed on the football helmet as well as the results from the processing methods selected. This chapter is divided into five sections, where the first discusses the acoustic test results and the application of Fourier Transform methods to the data in post-processing. Results for the first round of validation tests are presented in the second section. The third section discusses the differences between the STFT for impact points on the crown of the helmet and the fourth section compares the STFT results for impact points relative to their neighbors for one microphone. The final section discusses an evaluation using the single-number metrics of Kurtosis for both frequency and time-domain and RMS for the time-domain acoustic signals.

4.1 Raw Data Discussion

Raw acoustic data for both rounds of trials was collected into files and transferred into Matlab®. Additional tests using the sound calibrator revealed a difference in the pressure readings for the right microphone; the right microphone produced a lower pressure measurement amplitude than the left microphone for the same sound produced by the calibrator. This was corrected in post processing by recording the percentage difference between the reading for the left microphone and right microphone from the sound calibrator. The left microphone reading was approximately 18% higher than the right microphone reading. This correction is valid since the sensitivity of the microphone is a linear operation.

The application of the correction factor is simply a change of the sensitivity for the right microphone after measurement. Note that absolute pressure readings are not necessarily critical for these experiments since the process only makes relative comparisons between different data sets. The key is that the microphone sensitivities remain consistent throughout the experiment once they are set.

As explained in chapter 2, the Fast Fourier Transform and Short Time Fourier Transform are both applied to acoustic data. Appendix B contains several Matlab® codes that were written to perform Fast Fourier Transform (FFT) and Short Time Fourier Transform (STFT) analysis on the zero-averaged (background) acoustic data. Note that these are sample codes where specific changes were made based on what correlation was being investigated.

The m-file in Appendix B.4 works by using the built in fft command in Matlab®. The FFT is applied to both the left and right microphones for each impact point. The two-sided spectrum for each microphone is calculated and that is subsequently converted to a one-sided spectrum. The sampling frequency of the signal analyzer was 25,600 Hz. A frequency spectrum was created based on this sampling frequency when plotting the FFT for each impact point. The high end of the frequency range plot was truncated at 2,500 Hz since the energy density was mostly concentrated below that value. The results from using this code to evaluate linearity of the system is discussed in section 4.3.

The m-file in Appendix B.3 is the application of the Short Time Fourier Transform to the acoustic data. This code works in conjunction with the function file 'STFT' in Appendix B.2 to create the STFT plots for each impact point data set. The function file requires four input values: the time vector of the acoustic signal, the acoustic signal vector, the number of points to be used in the Short Time Fourier Transform, and the percentage of overlap between successive

transforms.

The input impulse for each force impact data point is calculated by summing the squared value of the measured force values over a time span that encompassed the complete pulse and taking the square root of that summation. A Hanning window is applied to each time set of data before applying the STFT. Then, the normalized STFT of the measured pressure for each impact point data set is calculated and subsequently divided by the associated impulse for that same impact location. This scaling helps to enable a more effective comparison between different data sets when the impact force level might be slightly different for each of those experiments. Since the interest here is in force location and not force magnitude, the effect of the force magnitude is essentially scaled out of the data. As noted above, the validation of the linear relationship between impulse level and measured acoustic signature is discussed in the next section.

The m-file 'Helmet_Analysis' then generates plots for the results of the analysis. This code allows results for up to ten impact locations to be compared in one master figure. Multiple parameters can be changed to suit the analysis at hand. The number of FFT points for each STFT can be changed, although it must remain an exponential power of two to retain the fast feature. The percentage of overlap between subsequent STFTs can also be changed, but for every case in this study the overlap value was 90%.

4.2 Validation Test Results

The first round of testing involved the examination of the relationship between the acoustic signature levels and the magnitude of the associated impulse. Figure 4.2.1 shows the measured force for each impact test performed in this validation test. As seen in the figure, there are three relative force levels delivered to the system: a soft impact, a medium impact and a hard/large impact. The impact locations are labelled according to the level of impulse imparted

and the impact location; each point is labeled with the section number on the helmet (*e.g.* 12), the letter of the point within that section (*e.g.* B), and either S, M, or L to designate a soft, medium, or large impact, respectively.

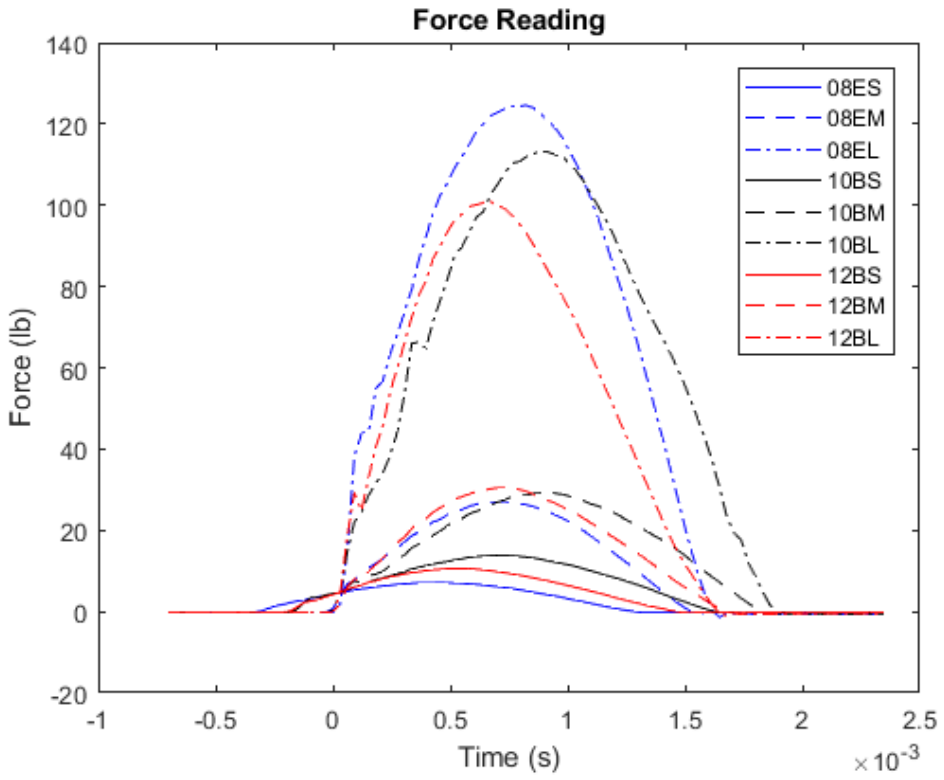

Figure 4.2.1. Measured force value for Validation Trials

The maximum magnitude of the small impacts ranged from 7-14 lb, the maximum magnitude of the medium impacts ranged from 27-30 lb, and the maximum magnitude of the hard impacts ranged from 100-124 lb. The plot in Figure 4.2.1 was truncated to show the curve of each impact over the same time duration. Each location is coded in one color: blue for location 08E, black for location 10B, and red for location 12B. All nine impacts in this test lasted less than two milliseconds. The magnitude of the impulse for each impact point is shown in Figure 4.2.2.

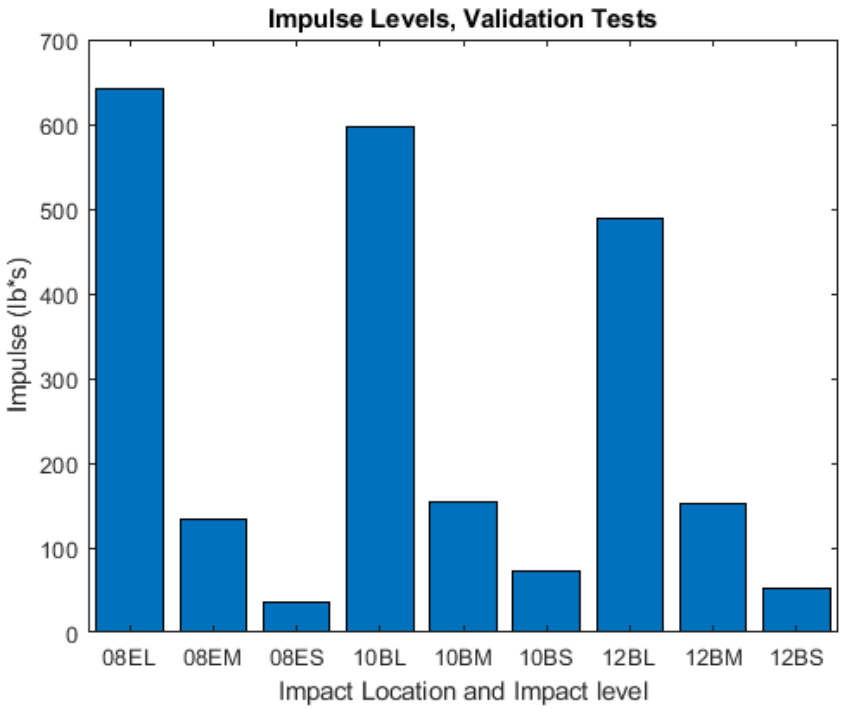

Figure 4.2.2. Impulse Levels for Validation Tests.

The different levels of impulse were not intended to be very precise, but rather to impart impulse at a certain order of magnitude. Since each impact location is compared only against itself, the exact value of the impulse magnitude for each level of impact is not important.

Figure 4.2.3 shows a time-domain plot of the acoustic signals recorded from the left microphone for the different impulse levels at impact point 8E. As expected, the pressure readings increase with the increase in impulse delivered.

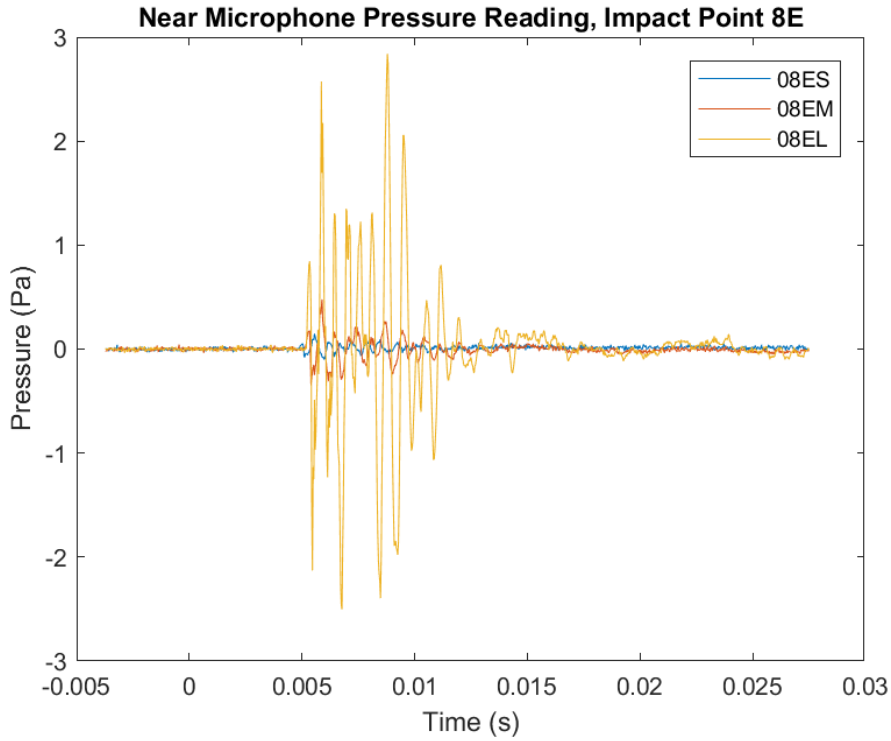

Figure 4.2.3. Time-domain Acoustic Signals for Left Microphone, Impact Point 8E.

Based on Figure 4.2.3, the acoustic radiation takes approximately five milliseconds after time passes 0 to reach the left microphone from impact point 8E. In theory, at a distance of roughly 6-6.5 ft (including the helmet size in this distance) with the speed of sound being 1125 ft/s, it would take an acoustic wave approximately 5-6 ms to reach the microphone, so the experimental and theoretical values agree and one can conclude as expected that these measurements are solely from the surface of the helmet.

Figure 4.2.4 shows the plots of the FFT spectrum of the left microphone pressure divided by the FFT spectrum of the force input. In this figure, each impact level is on one row of the figure, with all subplots in a column corresponding to impact location. The frequency amplitude is on a logarithmic scale for each subplot. While each impact location has a similar frequency spectrum for each force level, the amplitudes for different impact levels are different despite

being normalized to the force spectrum. Note that the high frequency regions of these plots do contain more noise due the associated low force amplitudes in these regions, which is discussed next. Figure 4.2.5 shows that the frequency spectrum for the force for the different impact levels varies in magnitude at each location, despite the shape of the frequency spectrum being similar for each point. The frequency amplitude is on a logarithmic scale for each subplot in this figure as well. This indicates that comparative analysis between impact locations must be done at a similar force level to obtain reasonable results.

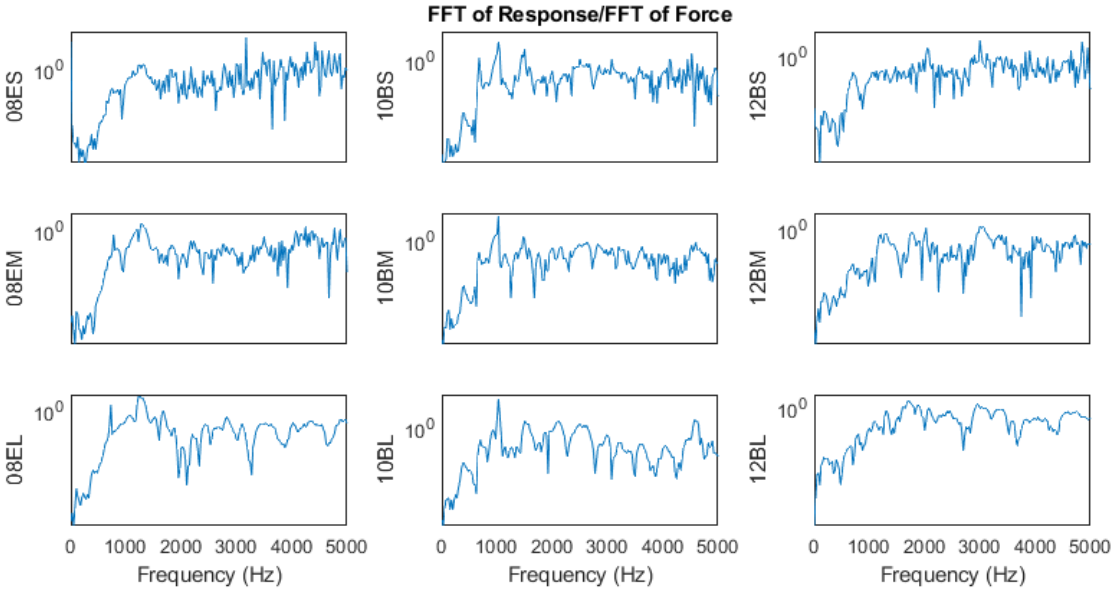

Figure 4.2.4. FFT of Left Microphone Response, Normalized to Force Spectrum.

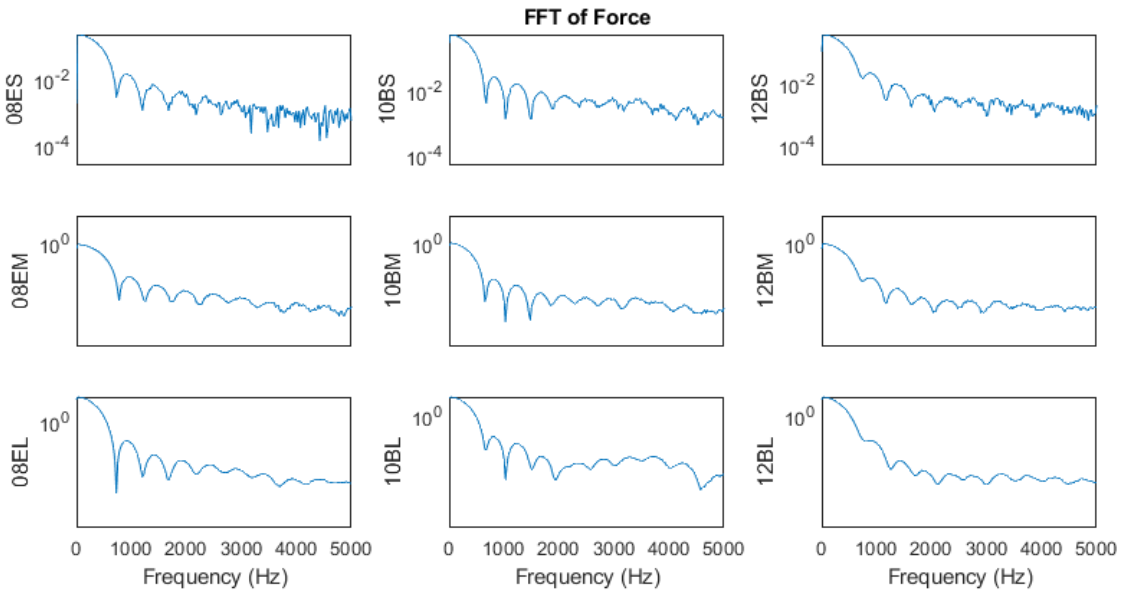

Figure 4.2.5. FFT Spectrum of Force.

Before comparing results for different impact locations to each other, it would be of interest to compare the acoustic radiation in different directions. The next section compares measurements at both microphone locations for chosen points along the center of the helmet.

4.3 Crown Point Comparison

This section compares the acoustic signature for impact points along the crown of the helmet, that is, along the hemisphere line of the helmet. Figure 4.3.1 shows the points chosen for this comparison on the helmet grid. The objective of this comparison is to examine if the symmetry assumption for the helmet's acoustic radiation, when excited along the helmet centerline, is valid.

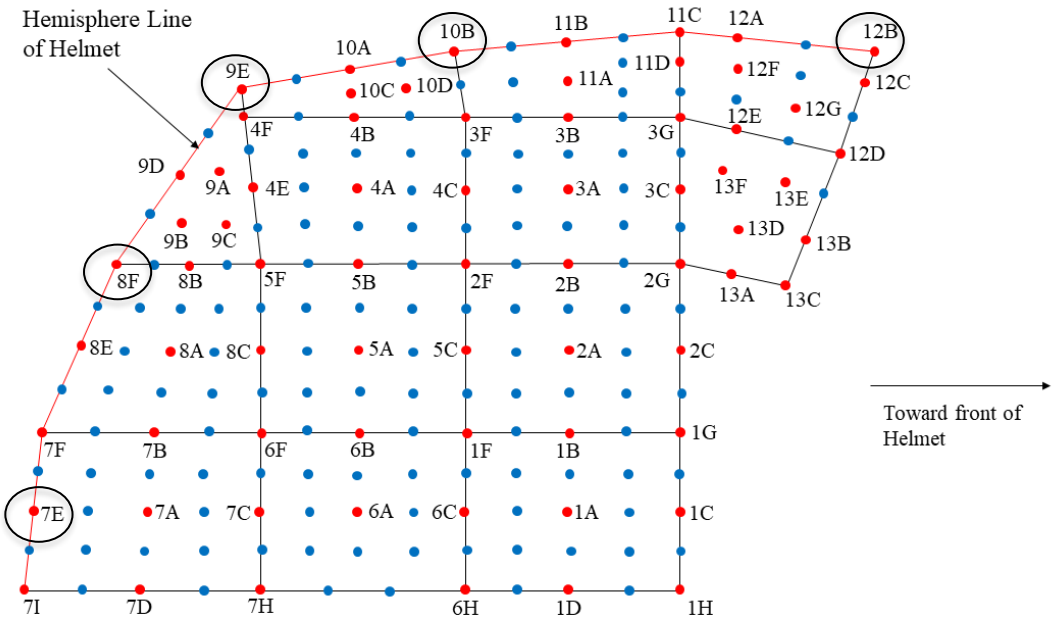

Figure 4.3.1. Crown points on the Helmet Grid.

As stated back in section 4.2, the acoustic signature for each point along the crown of the helmet is expected to be the same in the left and right directions, since the microphones are the same distance apart and assuming the helmet vibrates and radiates sound symmetrically. This premise does assume the helmet is perfectly symmetric, which may not be the case. No object is perfectly symmetric, and more importantly the physical attachments on the helmet are not symmetric. The foam padding inserted to protect the head of the player attaches to the polycarbonate shell via Velcro pieces. These pieces of Velcro are not identical, nor are they in the same position on both sides of the interior of the helmet shell. If these pieces of Velcro coincide with a node or anti-node on the shell of the helmet, it could change the vibration characteristics of the structure.

There are five impact locations along the crown of the helmet that were evaluated. Locations 7E, 8F, 9E, 10B, and 12B were the impact locations chosen. These points are circled

back in Figure 4.3.1. Figure 4.3.2 shows the STFT plots for the five impact locations chosen, where the plots for the left and right microphones at each impact location are next to each other to ease comparison.

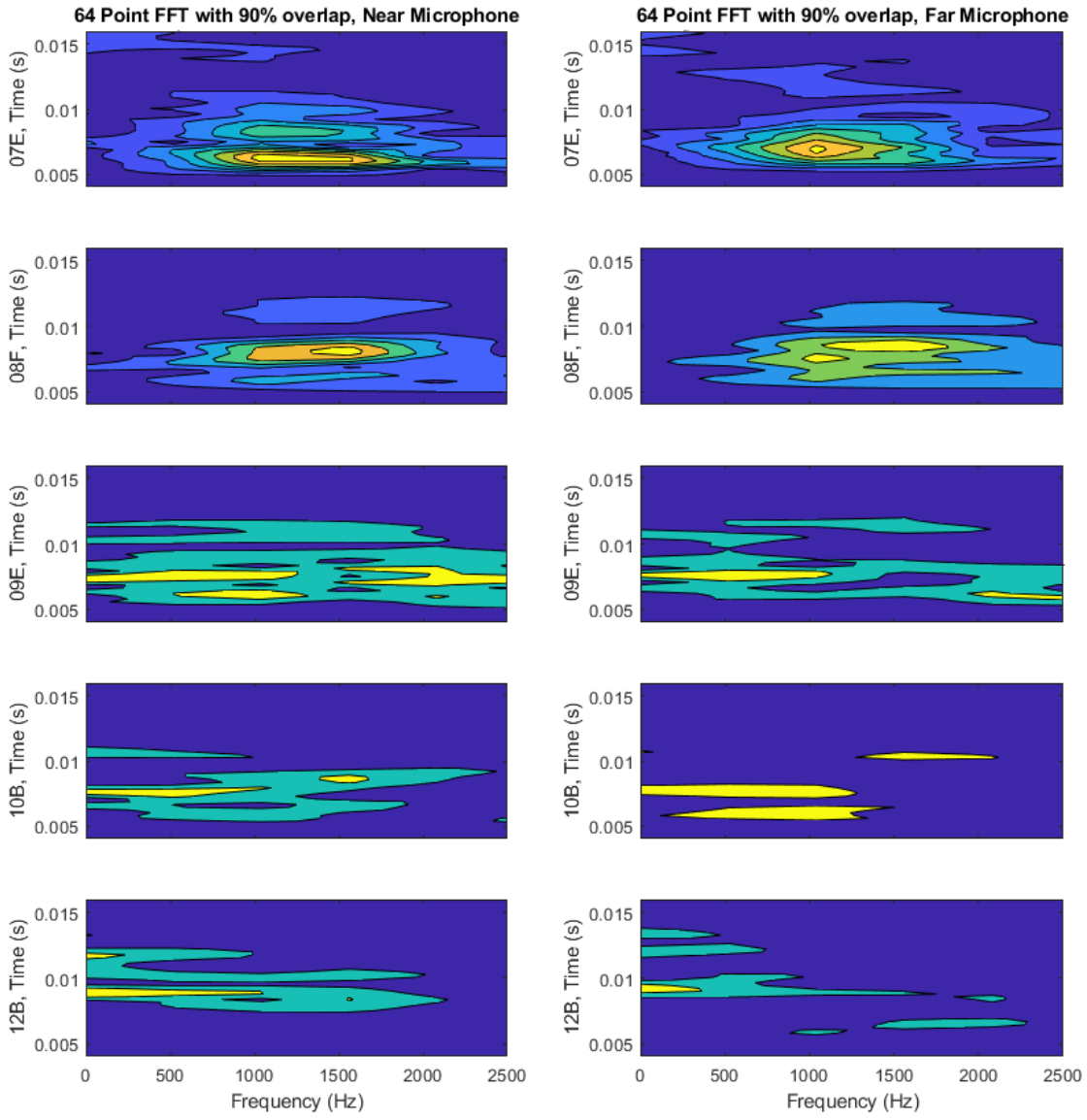

Figure 4.3.2. STFT Plots for five Crown locations.

As seen in the figure, the STFT plots for both microphones show similarities for all five impact locations. This is expected since both microphones are an equal distance away from each impact location and the pressure wave radiates almost symmetrically. Location 7E is located on

the backside of the helmet and has a frequency peak at about 1000 Hz that occurs at approximately 7 ms. The STFT bands for location 7E are slightly different as the right microphone does not show a band stretching to roughly 1500 Hz, but the general behavior recorded by both microphones is similar. Location 8F is located on the mid-upper back region and shows a frequency peak at about 1500 Hz that occurs at approximately 9 ms. Both microphones for this impact location show this frequency peak at the same point in time. The next impact location, point 9E, is located towards the back of the top region of the helmet. This location shows a frequency band that stretches from 0 Hz to roughly 1250 Hz that occurs at approximately 7.5 ms. Impact location 10B shows a similar band that occurs at approximately 8 ms. Location 10B is located on the top of the helmet. The frequency band amplitude for this point vary significantly. The final impact location on the crown 12B has a frequency band that stretches from 0 Hz to roughly 1000 Hz that occurs at about 9 ms. This band also varies in amplitude significantly between the readings for both microphones. Nevertheless, there is a relatively low frequency band that occurs at the same point in time (9 ms) for both measurements.

As stated previously, there are likely structural reasons why the STFT plots for the points examined above are not exactly the same. The vibration patterns in the helmet may be causing different patterns of acoustic radiation in different directions. It is also possible that there are non-symmetric vibration modes in the helmet which cause different acoustic radiation patterns in different directions. Although one might expect these modes to not be excited along the crown, the viscoelastic foam on the underside may be introducing a slight coupling component between the modes as well as introducing an anti-symmetry in the helmet's vibration pattern. Also, the impulse hammer may be causing a difference because of the slight difference in the angle for

each impact. If the hammer does not strike the helmet perfectly perpendicular to the surface, it may cause the acoustic pressure to radiate unevenly as a result of slightly different excitations in the modes. A possible third source of this difference comes from the human element. The experimenter was constrained to the area directly behind or in front of the test stand for each impact. If the experimenter's arm is held at an angle to hit a specific location, some of the acoustic energy could have been absorbed by the experimenter's arm and changed the magnitude of the frequency peaks shown in the plots.

4.4 Regional Point Comparison

After examining the symmetry of the acoustic radiation, the hypothesis of this work was tested by examining acoustic radiation changes for impacts at different locations within a region of the helmet. For this examination, three different regions of nine points were chosen on the side, back, and top of the helmet. The points were compared using the STFT plots from the readings collected at the left microphone. These STFT plots all use the same color scale and are all divided by their impact location's impulse magnitude to enable a relative comparison. The regional point comparison will continue in the next section with the discussion of single number metrics. The overall differences between impact regions will be compared as well as individual differences between locations within each region.

The first region chosen was on the side of the helmet. The layout for this impact region is shown in Figure 4.4.1. This region is centered at impact location 5C, and all locations are labeled in the figure. It is worth nothing that there is a large hole in the shell of the helmet near this region below location 1F and 1B. Location 2A is obscured by the chin-strap in Figure 4.4.1. Recall that this chin strap was removed for testing.

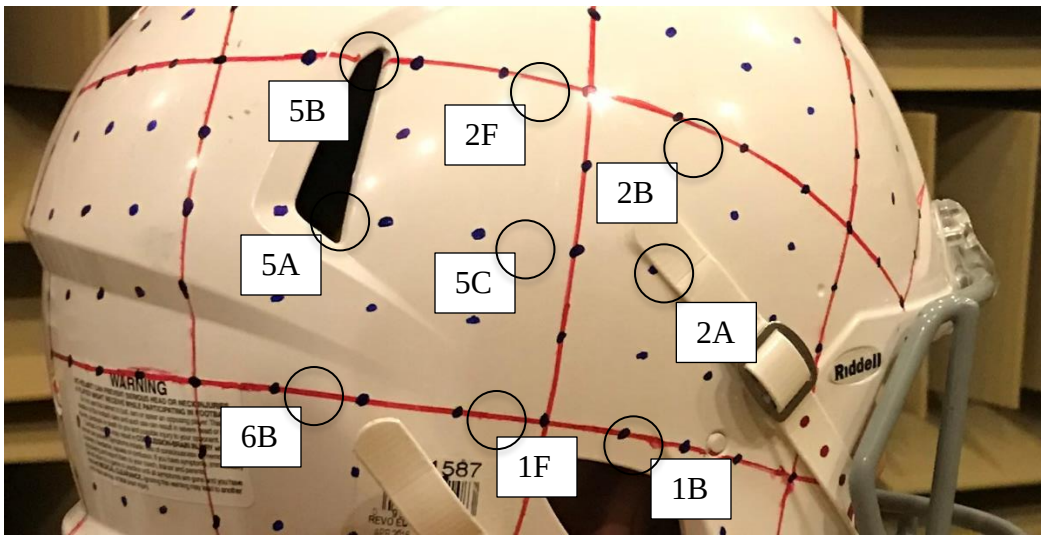

Figure 4.4.1. Impact Location Layout for Side Region.

Figure 4.4.2 shows the STFT plots for the nine locations for this region. Note that the subplot layout matches the impact location layout on the helmet surface. Each impact location, except points 6B and 1B, exhibits a frequency peak at roughly 1000 Hz that occurs at a time of approximately 8-9 ms. Location 5C has two frequency peaks near 1000 Hz that occur around 8 ms and 10 ms. Moving the impact location directly towards the front, back, top, or bottom of the helmet causes the peak at 10 ms to decrease significantly. However, moving the impact location towards the top and back to location 5B shows that this peak at approximately 10 ms reappears and dominates the acoustic response. At locations 6B and 1B towards the bottom of the helmet a higher frequency peak that occurs at 6 ms appears between 1500 and 2000 Hz. Despite these minor differences, all nine points in this region exhibit similar acoustic radiation characteristics. Still, there are slight differences in the STFT points that indicate that it may be possible to use such a technique for identifying impact location.

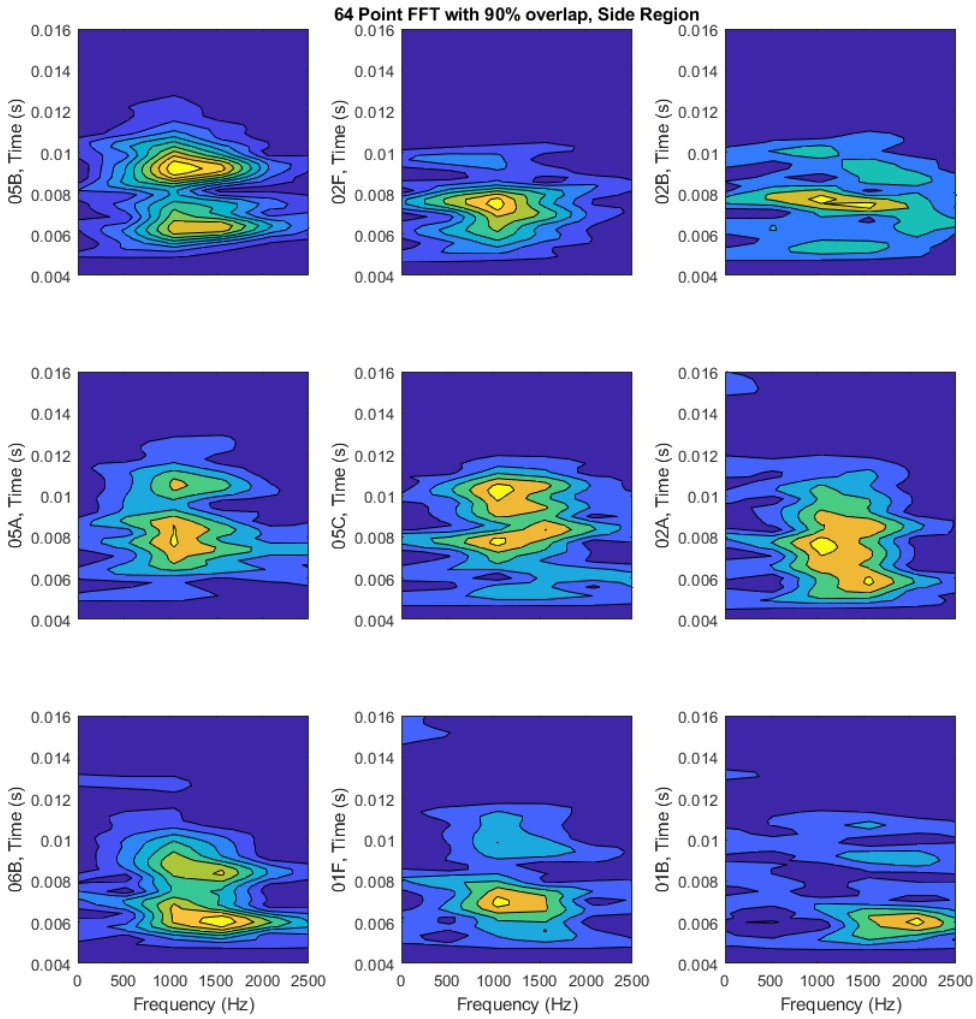

Figure 4.4.2. STFT Plots for Side Region Impact Locations.

The second impact region chosen was on the back of the helmet. The geometry for this region is shown in Figure 4.4.3. This region is centered at location 7B, and all locations are labeled in the figure. Between the line of points 7F, 7B, and 6F and the line of points 8E, 8A, and 8C there is a significant geometry feature where the helmet has a ridge.

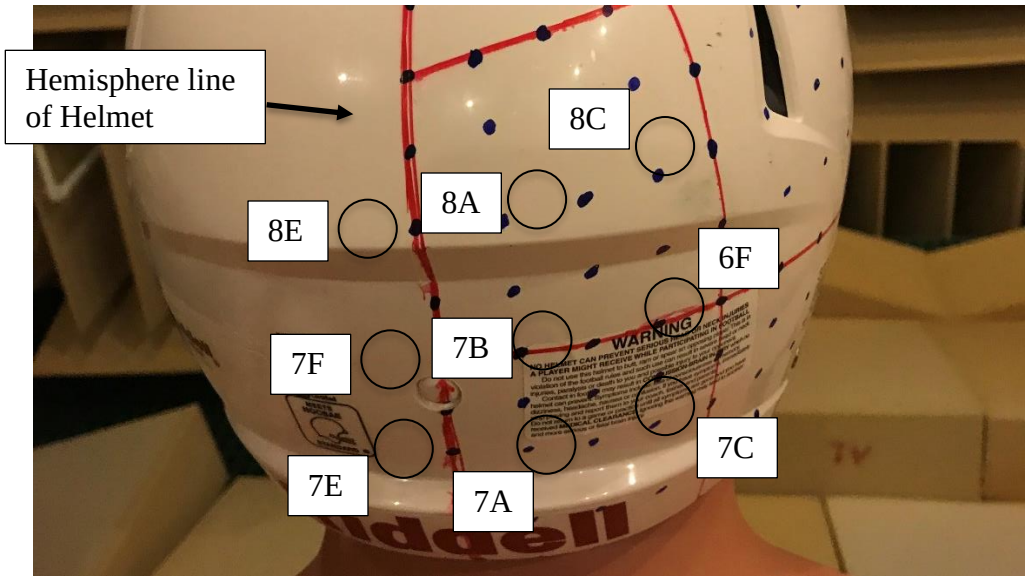

Figure 4.4.3. Region Geometry for Back Region.

Figure 4.4.4 shows the STFT plots for the nine locations chosen for this region. Again, the plot layout matches the impact location layout. These locations exhibit significant differences between their acoustic signatures. Location 7E exhibits a relatively wide frequency peak from around 1000 to 1500 Hz at around 6 ms, which disappears from the response for locations 7F and 7A immediately above and next to location 7E. However, there is a secondary peak at about 8 ms for location 7E that grows in magnitude moving along the hemisphere line to locations 7F and 8E. Between the line of locations 7F, 7B, and 6F and the line of locations 8E, 8A, and 8C a significant change occurs and the STFT plots look drastically different. This might be explained by the ridge seen in Figure 4.4.3 between the line of locations 7F, 7B, and 6F and the line of locations 8E, 8A, and 8C. This ridge may cause vibrations to radiate differently throughout the structure which would cause a significantly different acoustic response. In general, the excited frequency bands in this region are broader and more smeared than for the previous region discussed above.

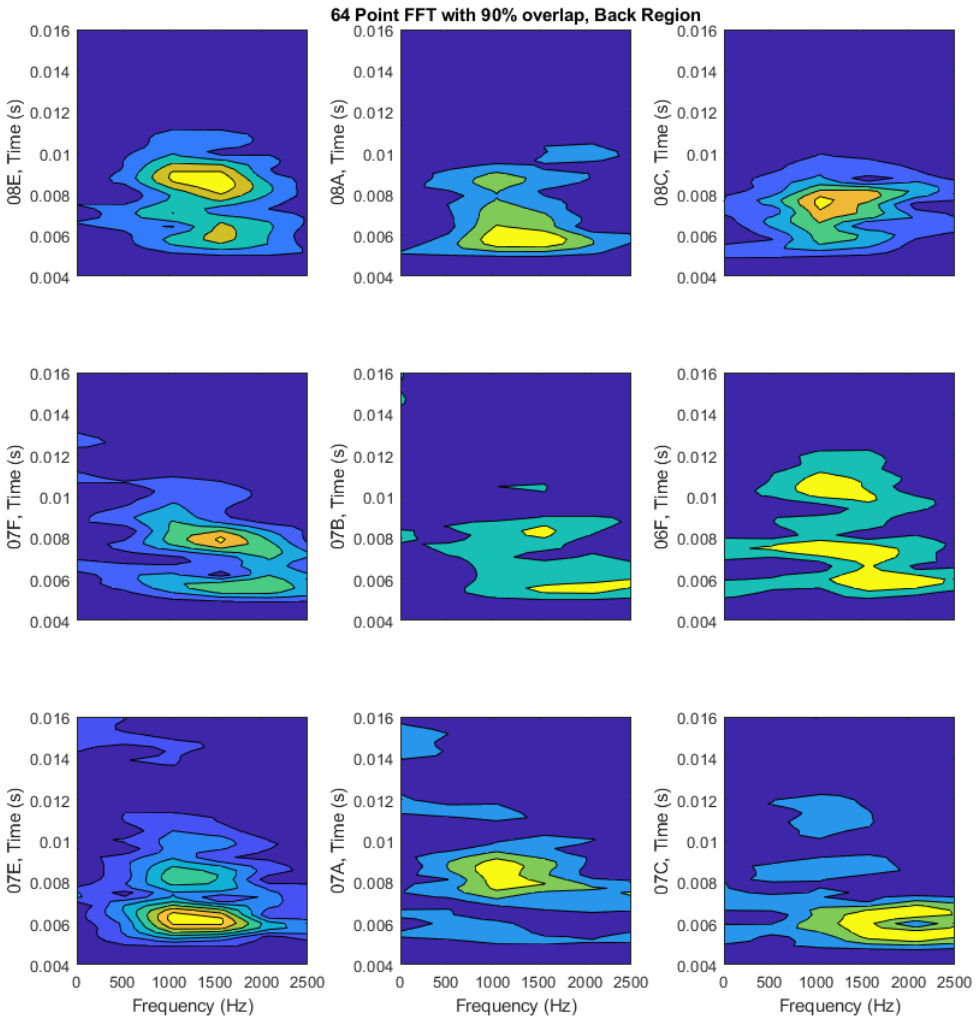

Figure 4.4.4. STFT Plots for Back Region Impact Locations.

The final region chosen was on the side of the helmet. The geometry for this region is shown in Figure 4.4.5. This region is centered at impact location 10D, and all locations are labeled in the figure.

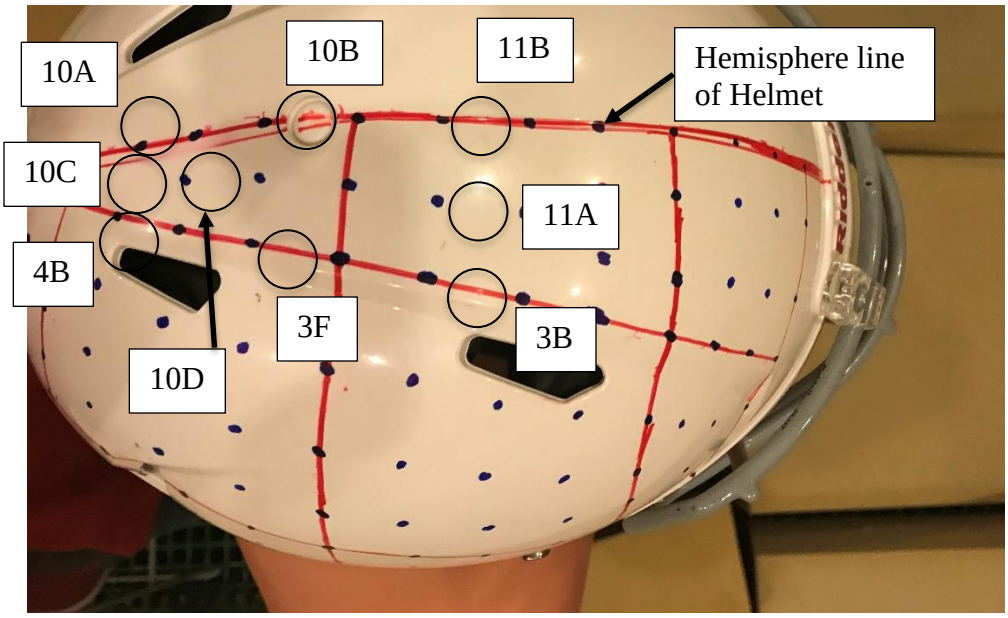

Figure 4.4.5. Region Geometry for Top Region.

Figure 4.4.6 shows the STFT plots for the nine locations chosen for this region. While the plot layout generally follows the impact location layout, note that the plots in the center column do not have impact locations along a line. These locations also exhibit significant differences between their acoustic signatures, but not as extreme as the locations in the region on the back of the helmet shown back in Figure 4.4.3. Impact at locations 10D, 11A, 3F, and 3B result in frequency peaks at around 1500 Hz that occur at approximately 8 ms. This peak is also seen for locations 4B and 10C, but these locations also have an additional peak at roughly 1500 Hz that occurs between approximately 9 and 10 ms. These two peaks are also present in the response for location 10A, but they have a smaller amplitude. Of the three regions considered, this region appears to have the least variation in STFT with impact location throughout that region.

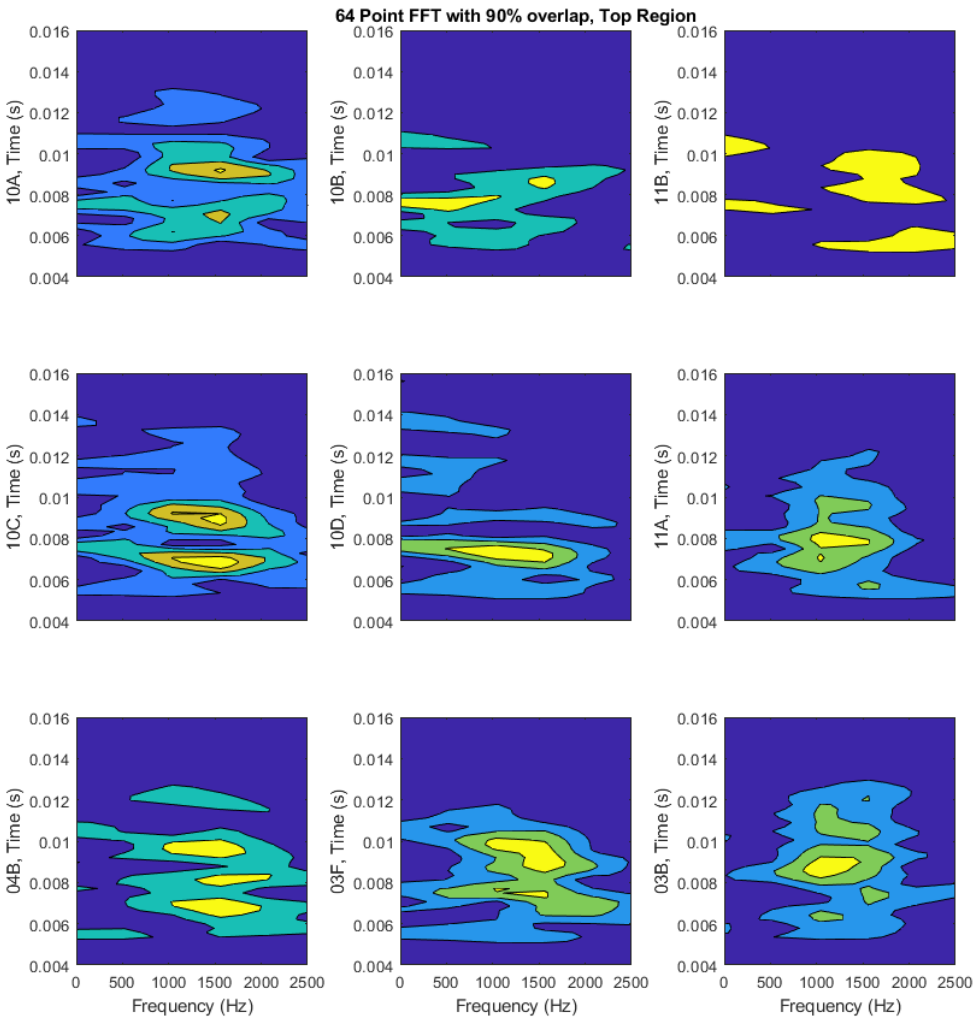

Figure 4.4.6. STFT Plots for Top Region Impact Locations.

The three regions analyzed here show similarity in the acoustic response for locations within the region, but there is enough differentiation between the acoustic signature for some locations that this approach could possibly be used to identify an impact location or a more general impact region. However, this method would be tedious to implement due to the volume of data presented in these results. It is possible that an image analysis algorithm could analyze the STFT plots to infer a regional impact location, but a simpler method is highly desirable. The next section discussed such approaches in the single number metric analysis.

4.5 Evaluation of Single-Number Metrics

As explained in chapter 2, one of the objectives of the research is to examine the use of single number metrics in potentially identifying the location of an impact. The Absolute Kurtosis (AK) of a signal is a measure of the peaks within a signal. The AK for the acoustic response of each point to an impact was calculated for the normalized FFT of the acoustic signal recorded at the left microphone. The FFT was normalized by dividing the response spectrum by the force spectrum. The same regions defined in section 4.4 are used here for analysis. Figure 4.5.1 shows the AK values for the side region as defined back in Figure 4.4.1.

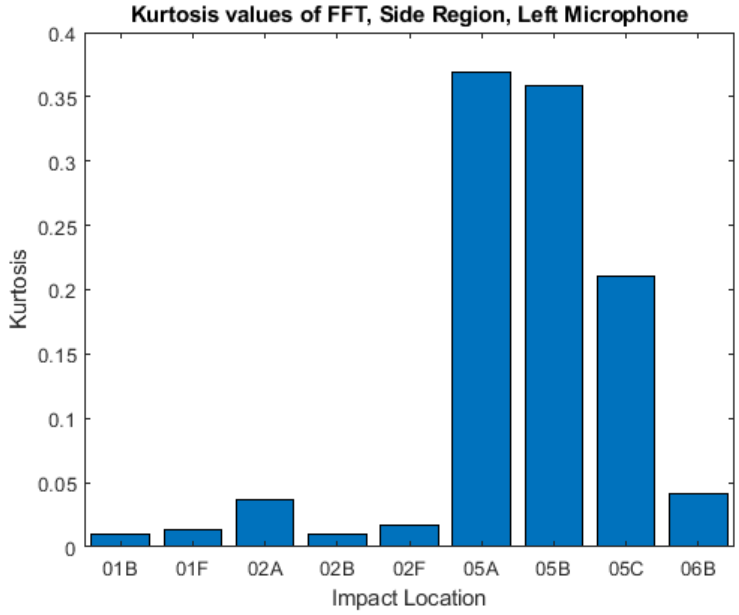

Figure 4.5.1. Absolute Kurtosis, Left Microphone FFT, Side Region.

There appear to be some locations within this region that could be identified using the AK values. Location 5C has a unique AK value which could allow that location to be identified via this processing method. Locations 5A and 5B have much higher AK values, but the small difference in AK between these two locations means this metric would not be able to distinguish between these impact locations. Of course, it may be possible to identify an impact within a

region around those two locations. For the other impact locations within this region, it would be difficult to differentiate locating using AK.

Figure 4.5.2 shows the AK values for the back region as defined back in Figure 4.4.3. Figure 4.5.2 shows precision locations 7A, 7B, 7C, 7E, and 7F; these locations would not be easy to distinguish using this metric. However, location 8A exhibits much lower AK value than the rest of the locations in this region. Location 8A could likely be identified using this metric.

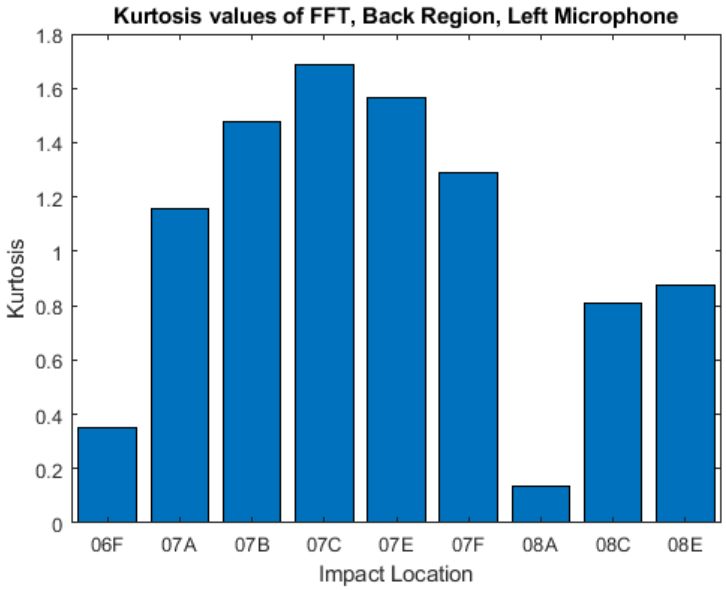

Figure 4.5.2. Absolute Kurtosis, Left Microphone FFT, Back Region.

Figure 4.5.3 shows the AK values for the top region defined back in Figure 4.4.5. The AK values for this region separate the locations into two main groups. Locations 10A, 10B, 10C, and 10D are likely indistinguishable from each other, and locations 3B, 3F, 4B, and 11B are also likely indistinguishable from each other. Location 11A has a unique AK which could allow it to be distinguished from the other locations. The precision between clusters of locations means that small regions for the impact location may be inferred, but specific points would likely not be able to be identified.

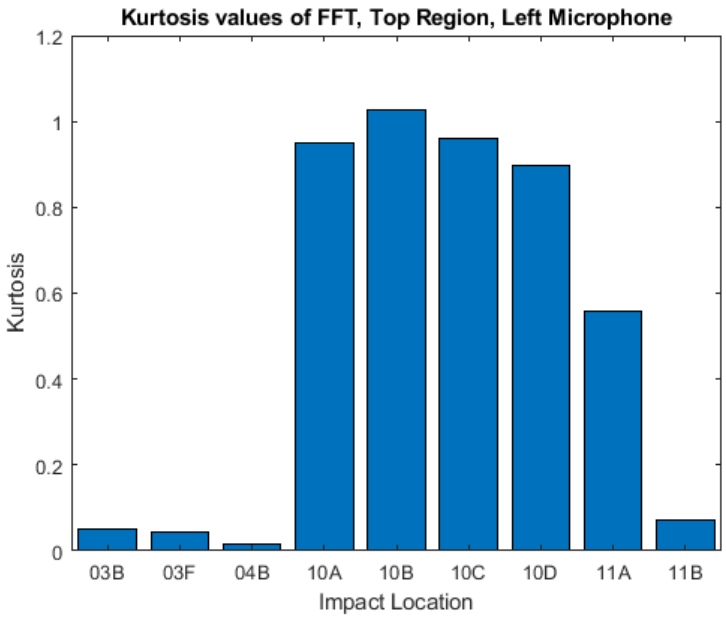

Figure 4.5.3. Absolute Kurtosis, Left Microphone FFT, Top Region.

The dissimilar values for the frequency-domain AK values in each region indicates that this metric could be used to identify certain impact locations on some parts of the helmet, but only more general impact regions on other parts of the helmet. Some locations have very similar AK values that inhibit distinguishing between the locations.

AK was also calculated for the time-domain signals at the locations in each of these three regions, however there were no identifiable features that would allow this metric to distinguish impact locations. Since the AK values for the time-domain response lacked any clear relationship with the acoustic response, the results of the AK time-domain values are not shown.

Another analysis method considered is the Root-Mean-Square (RMS) analysis. For this approach, the time-domain signals for the 27 locations defined for the side, back, and top region in section 4.4 are divided by their respective impulse values for the associated force, which is just a single value for each impact. The RMS value of the pressure signal for each impact

location is calculated via the method outlined in section 2.4. Figure 4.5.4 shows the RMS values for the impact locations in the side region defined back in Figure 4.4.1.

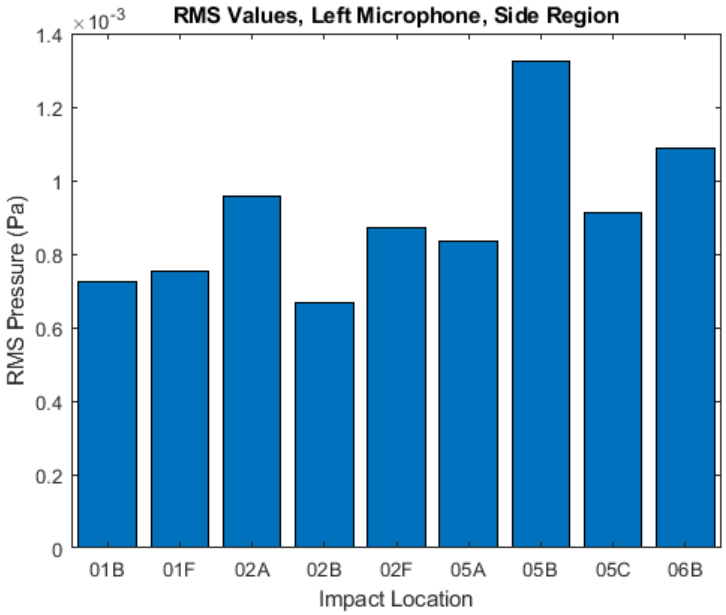

Figure 4.5.4. RMS Pressure Values, Left Microphone, Side Region.

Figure 4.5.4 shows that the RMS pressure values are similar. The RMS pressure tends to increase towards the center of the helmet, closer to location 5B. Clearly location 5B is identifiable within this region.

Figure 4.5.5 shows the RMS values for the impact locations in the back region defined back in Figure 4.4.3, and Figure 4.5.6 shows the RMS values for the impact locations in the top region defined back in Figure 4.4.5.

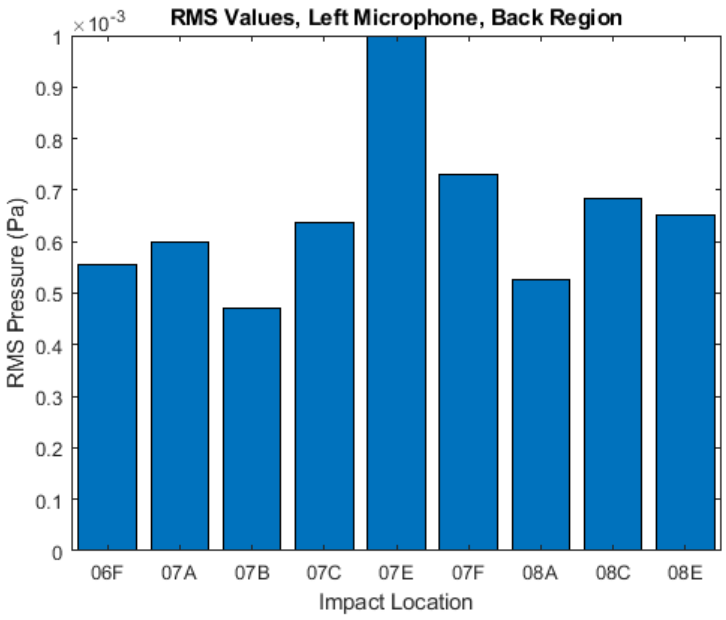

Figure 4.5.5. RMS Pressure Values, Left Microphone, Back Region.

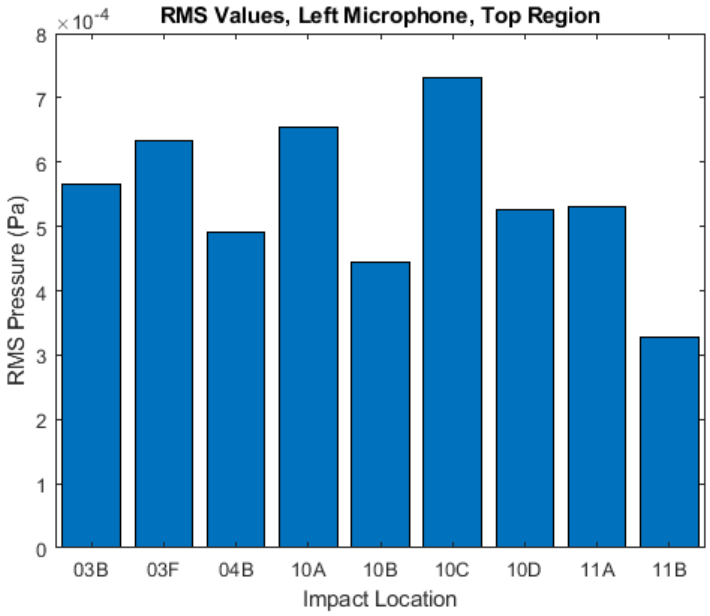

Figure 4.5.6. RMS Pressure Values, Left Microphone, Top Region.

Figure 4.5.6 shows lower average RMS pressure values for the top region than the average RMS pressure for the other two regions. The RMS pressure values in Figure 4.5.5 are fairly similar with the RMS pressure values in Figure 4.5.4, meaning that the RMS pressure for

the side and back regions are mostly indistinguishable except for a few locations. This could be due to the way the vibration modes are not excited as well when the helmet is impacted towards the top. It is possible these locations are closer to node lines for the vibration modes, and that the impact does not cause the sides of the helmet, which are closer to the microphones, to vibrate as much.

Based on the results in this section, RMS pressure seems like a potential metric for inferring a region that the impact may be located within, while AK is a better metric for determining the specific location the impact occurred at within that region. However, it does appear that AK only works if the locations have a specific distance between them. Otherwise the AK appears too similar to distinguish specific impact locations.

4.6 Concluding Remarks

This chapter presented the results of the signal processing methods used. The FFT results showed a somewhat linear relationship between impact force level and the frequency spectrum of the acoustic response. The STFT results revealed a nearly symmetric acoustic signature for impact points along the helmet crown, and could be used to infer impact location, although this would be a tedious process. The single-number metrics RMS and AK showed good ability to regionalize an unknown impact location. The next chapter presents the conclusions of this thesis as well as recommendations for future work.

CHAPTER 5

CONCLUSION

This chapter discusses conclusions related to the results of the experiments and processing methods and is divided into two sections. The first section presents the conclusions of this study and the second section includes recommendations for future work.

5.1 Conclusions

Acoustic methods for regionalizing an impact force have been presented. It was shown that higher impulse levels result in a different FFT frequency spectrum for the input force. As a result, it was determined that comparisons between locations on the helmet could only be done for impulse levels of a similar range.

The acoustic response was measured in two directions for locations along the hemisphere line of the helmet and the STFT method was used to compare the acoustic signature in both directions. It was determined that the acoustic signature in both directions is nearly symmetrical for locations along the hemisphere line of the helmet. There were slight differences in the radiation to the right of the helmet versus the left, and these differences were believed to result from non-symmetric vibration modes being excited by the impact.

The STFT method was used to analyze the response in three regions of the helmet. For each region, the STFT plots showed some common frequency features. However, the results for some locations had differentiating features making STFT a valid method for determining some regional impact locations, but this method was concluded to be too tedious to implement well.

Two single-number metrics were presented as methods for regionalizing impact locations: Kurtosis and RMS. Kurtosis showed an ability to distinguish certain impact locations within regions, but there was a limit to this differentiation. In some regions, groups of impact locations had similar AK values making them indistinguishable from each other by this metric. Normalized RMS pressure showed consistency among values in each particular region. The RMS pressure metric could be used to infer a general area of the helmet where an impact is located, while the AK is a better method for determining a specific impact location.

From these experimental results, it is clear that further investigation of acoustic methods for force location identification is needed. Other methods will need to be considered to examine correlations between impact location and measured acoustic response.

5.2 Recommendations for Future Work

The acoustic methods presented in this thesis show a correlation between the impact location on a structure and the acoustic radiation, but there is room for further investigation. A prime area of investigation would be into the repeatability of the results presented here. Future research should examine the acoustic signature for repeatable impact loads at different locations to examine how or if the acoustic signature changes.

The STFT plots for locations near each other showed many similarities, but changing locations by small amounts changes the acoustic radiation characteristics, which helps distinguish each impact locations from its neighbors. However, the AK values for certain points were very similar, meaning that AK could not be used to differentiate between these impact locations. As only a few specific locations could be identified, the distance between locations at which the AK values begin to vary significantly should be investigated further. It is also recommended that cross-correlation techniques be applied to the STFT results to examine if it

would be possible to determine other single-number metrics that are useful in identifying impact location.

Another avenue for future research is in evaluating the relationship between the vibration characteristics of a structure excited by impact and the measured acoustic response. This study postulated non-symmetric vibration modes as a potential cause for non-symmetric acoustic radiation, but this was not verified through any measurement or modeling. Finite element modeling for a complex structure may prove difficult, but an FEA model of the structure would be the first step in building a more complete analysis. The vibration characteristics could be determined through a non-contact measurement method such as laser doppler vibrometry. The other piece of an acoustic inverse method would be building a model of the acoustic environment. This would be extremely difficult, but bears investigation to determine the feasibility of using acoustic inverse methods.

It is also recommended that future research investigate repeatability of the results obtained in this study. The impacts in this study were all of different magnitudes, and the frequency spectrum of each impact varies. It would be useful to examine the acoustic response for several impact locations subjected to a repeated, constant impulse magnitude impact force. If the hammer is used in future experiments, the repeatability of the associated acoustic signature should be examined by striking the helmet multiple times at a single location and noting any changes in the measured signature. These issues could be eliminated entirely be removing the human component and developing some electro-mechanical method of impact excitation. This could be done by developing a source that produces a repeatable force of short duration that can be moved around the inner surface of the helmet. It would also be desirable to examine how

different helmets of the same model respond to the same impulse at the same location on each helmet, to examine the uniqueness of the acoustic radiation from an impact location.

It is further recommended that the research presented here be repeated with more microphone locations to measure the acoustic radiation in more than two directions. Possible configurations could include microphones above and below the helmet as well as in front and behind the helmet to accurately map the acoustic response of the structure in three dimensions.

REFERENCES

Avitabile, P. “Why you can't ignore those vibration fixture resonances,” *Sound and Vibration*, 33(3), pp. 20-26 (1999).

Beckwith, J.G., Greenwald, R.M. & Chu, J.J. Ann Biomed Eng (2012) 40: 237. https://doi.org/10.1007/s10439-011-0422-2

Brigham, E. O. *The Fast Fourier Transform*. Prentice-Hall, 1974.

Buckberry, C, et al. “The Application of High-Speed TV-Holography to Time-Resolved Vibration Measurements.” *Optics and Lasers in Engineering*, vol. 32, no. 4, 1999, pp. 387–394., doi:10.1016/s0143-8166(00)00011-7.

Craun, Matthew A., and David Feit. “Comparison of matched-Field and pseudo-Inverse methods for source identification on a frame structure.” *Proceedings of the ASME Noise Control and Acoustics Division - 1999*, 1999, pp. 375–382.

Finch, Robert D. *Introduction to Acoustics*. Pearsen Prentice Hall, 2005.

Fabunmi, J. A. “Effects of Structural Modes on Vibratory Force Determination by the Pseudoinverse Technique.” *AIAA Journal*, vol. 24, no. 3, 1986, pp. 504–509., doi:10.2514/3.9297.

Greussing, D., et al. “The Conception of Structure-Borne-Sound-Based near-Field Holography.” Journal of Sound and Vibration, vol. 331, no. 18, Elsevier BV, Aug. 2012, pp. 4132–4144. Crossref, doi:10.1016/j.jsv.2012.04.022.

Hansen, P. C., “Regularization Tools: A Matlab Package for Analysis and Solution of Discrete Ill-posed Problems,” (2001).

Kaltenbach, Hans-Michael. *A Concise Guide to Statistics*. Springer, 2012.

Keller, J. A. “*A dictionary of terms for machinery diagnostics of gearboxes*,” US Army RDECOM, AED, Redstone Aresenal, AL.

Kinsler, Lawrence E., et al. *Fundamentals of Acoustics*. Wiley, 2000.

Kreyszig, Erwin, et al. *Advanced Engineering Mathematics*. John Wiley, 2011.

Liu, Yi, and W.Steve Shepard Jr. “An Improved Method for the Reconstruction of a Distributed Force Acting on a Vibrating Structure.” Journal of Sound and Vibration, vol. 291, no. 1–2, Elsevier BV, Mar. 2006, pp. 369–387. Crossref, doi:10.1016/j.jsv.2005.06.013.

Liu, Yi, and W.Steve Shepard Jr. “Dynamic Force Identification Based on Enhanced Least Squares and Total Least-Squares Schemes in the Frequency Domain.” Journal of Sound and Vibration, vol. 282, no. 1–2, Elsevier BV, Apr. 2005, pp. 37–60. Crossref, doi:10.1016/j.jsv.2004.02.041.

Liu, Yi, and W.Steve Shepard. “Reducing the Impact of Measurement Errors When Reconstructing Spatial Dynamic Forces.” Journal of Vibration and Acoustics, vol. 128, no. 5, ASME International, 2006, p. 586. Crossref, doi:10.1115/1.2202162.

Peterson, A. P. G. *Handbook of Noise Measurement*. GenRad, 1980.

Rao, Singiresu S. *Vibration of Continuous Systems*. John Wiley & Sons, 2007.

Thite, A.N., and D.J. Thompson. “Selection of response measurement locations to improve inverse force determination.” *Applied Acoustics*, vol. 67, no. 8, 2006, pp. 797–818., doi:10.1016/j.apacoust.2006.01.001.

Tongue, Benson H. *Principles of vibration*. Oxford University Press, 2001.

APPENDIX A

This appendix provides a larger version of the unwrapped helmet grid shown in Figure 3.2.2. The red dots represent locations impacted on the helmet and blue dots represents other mapped locations on the helmet that were not measured. The larger version of the helmet grid in found on the next page.

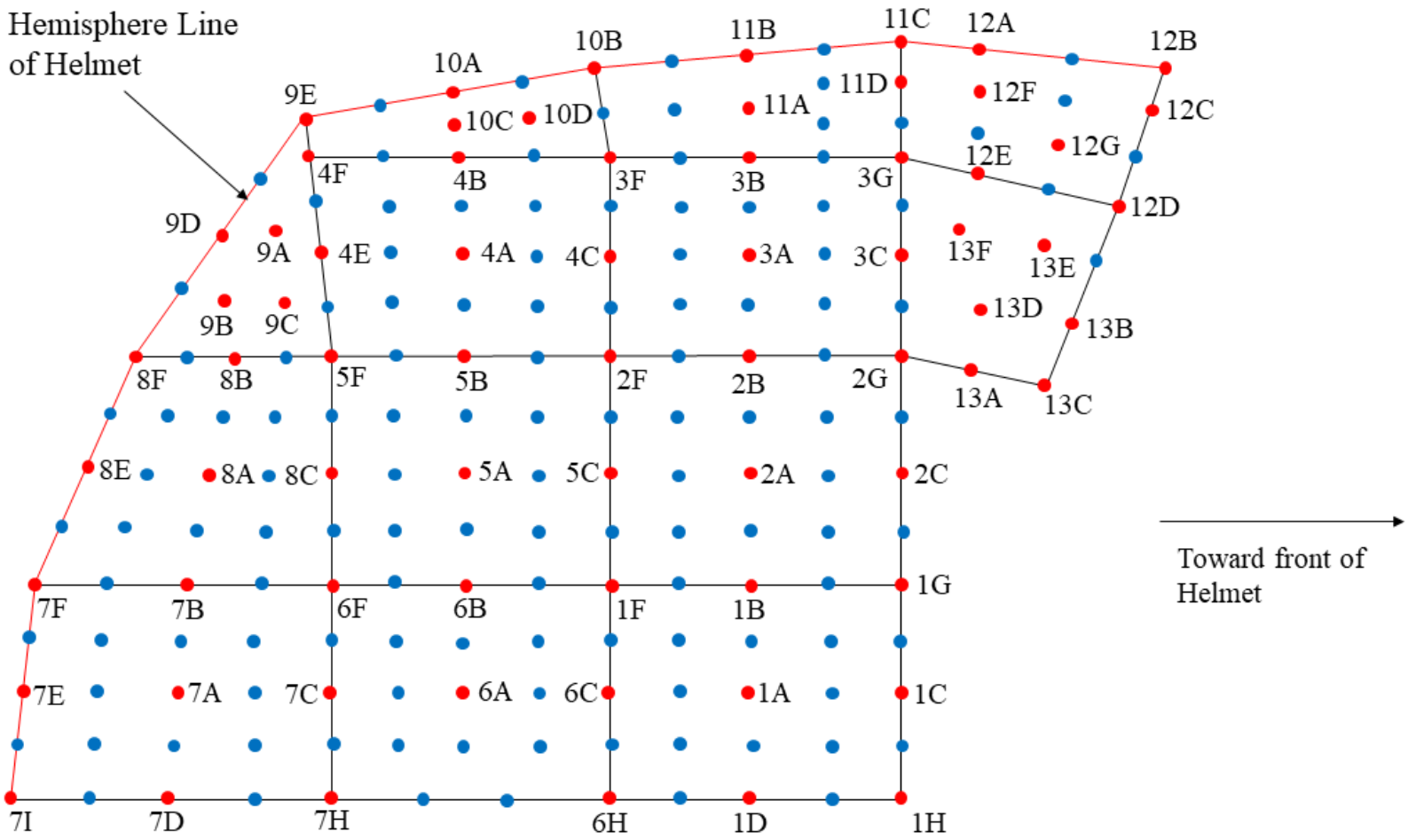
Hemisphere Line
of Helmet
9E
10A
10B
11B
11C
12A
12B
10C
10D
11A
11D
12F
12C
12E
12G
4F
4B
3F
3B
3G
12D
9D
9A
4E
4A
4C
3A
3C
13F
13E
9B
9C
13D
13B
8F
8B
5F
5B
2F
2B
2G
13A
13C
8E
8A
8C
5A
5C
2A
2C
Toward front of
Helmet
7F
7B
6F
6B
1F
1B
1G
7E
7A
7C
6A
6C
1A
1C
7I
7D
7H
6H
1D
1H

APPENDIX B

This appendix shows the MatLab codes used for processing the acoustic data.

B.1 Zero-Averaged Data

```
% Acoustic Helmet Data Correction
% (c) 2018 Jacob Davis

clear
load RawOrganizedDataV2.mat

% To correct the far microphone for the incorrect sensitivity

CH3 = CH3/-1.184811838045040;

% To Zero-average the Data

for k=1:70
    CH2(:,k) = CH2(:,k)-mean(CH2(1:254,k));
    CH3(:,k) = CH3(:,k)-mean(CH3(1:254,k));
end

% Plot Crown Point for Comparison

figure(8)
plot(Press_time,CH2(:,50),Press_time,CH3(:,50))
xlabel('t')
ylabel('Pa')
title('Point 12A Pressure reading')
legend('CH2','CH3')

clear k

save FullCorrectedDataV2.mat
```

B.2 STFT Function File

```
function [ stft_freq,stft_time,stft_spectrum ] =
STFT(time,value,numpts,overlap)
% STFT - Performs Short-Time Fourier Transform for a specified
number of
% points and a specified percentage of overlap between
successive FFTs.
% Besides values, output also generates two plots.
%
% STFT(time,value,numpts)
% Input:   time:     time vector for data (seconds)
%          value:    data values corresponding to each time
vector point
%          numpts:   number of points to execute Fourier
Transform
%                   (should be equal to 2^N for FFT)
%          overlap: overlap percentage (0-100) between
successive FFTs
%
% Output:  [stft_freq,stft_time,stft_spectrum]
%           stft_freq:     frequency values for the FFT
%           stft_time:     time value at the center of the data
window
%           stft_spectrum: frequency amplitudes


% Convert overlap percentage to an integer number of points
noverlap=floor(numpts*overlap/100);

% Do not allow 100% overlap
if noverlap==numpts,
    noverlap=noverlap-1;
end

% Compute number of times to execute FFT
ntimes=floor((length(time)-numpts)/(numpts-noverlap))+1;

% Initialize stft_spectrum array with zeros to speed execution
stft_spectrum=zeros(ntimes,numpts);

% Compute sampling frequency for use in frequency calculation
sample_freq=1/(time(2)-time(1));

for j=1:ntimes,
    % Determine index range of array for this particular FFT
```

```
    index_start=(1+(j-1)*(numpts-noverlap));
    index_end=index_start+numpts-1;
    % Find approximate (mean) value for time at center of index
range
    stft_time(j,1)=mean(time(index_start:index_end));
    % Compute FFT over specific index range
    % Apply a Hanning window to reduce effects of non-
periodicity

stft_spectrum(j,:)=abs(fft(value(index_start:index_end).*hann(in
dex_end-index_start+1)))/numpts;
end

% Determing frequencies for FFT values
stft_freq=sample_freq*linspace(0,1,numpts);

% Determine how many points are in half of FFT, since half is
aliased
num_fft=(length(stft_freq)/2+1);

% Since spectrum is symmetric and half is aliased, truncate to
half
stft_freq=stft_freq(1:num_fft);
stft_spectrum=stft_spectrum(:,1:num_fft);
```

B.3 STFT Plots

```
% Helmet_Analysis_64.m
%  For 64 point FFT

clear
load FullCorrectedDataV2.mat

% Find helmet impact force energy for points 50 through 400
Impulse=sqrt(sum(CH1(50:400,:).^2));

maxfreq=2500;
timeratio=1;

% Find 64 point spectrums with 90% overlap
for j=1:70

[Freq_64,Time_64,Spec_64(j,:,:)]=STFT(Press_time,CH2(:,j),64,90)
;
    NSpec_64(j,:,:)=Spec_64(j,:,:)/Impulse(j);
```

```
end

max_Spec_64=.0014;
%max_Spec_64=max(max(max(NSpec_64)));

figure(1)

for k=1:10
    Z(:,:)=NSpec_64(k,:,:);

subplot(5,2,k);C=contourf(Freq_64,Time_64,Z,[0:max_Spec_64/10:ma
x_Spec_64]);
    axis([0 maxfreq .004 .016]);
    if(k>8)
        xlabel('Frequency (Hz)');
    else
        set(gca,'XTickLabel','')
    end
    if(k<3),title('64 Point FFT with 90% overlap');end
    ylabel([datalabel(k,:),', Time (s)']);
    %print('1A-2C','-dpdf','-bestfit')
    %saveas(gcf,'1A-2C.fig')
end

clear Z;
```

B.4 FFT Analysis

```
% FFT Analysis of Acoustic Data
% (c) 2018 Jacob Davis

clear
load FullCorrectedDataV2.mat

% Find helmet impact force energy for points 100 through 200
Impulse=sqrt(sum(CH1(100:200,:).^2));

L=1024;
H=hann(L);

% Compute FFT for each Impact Location

for k=1:70
    CH2c(:,k)=H.*CH2(:,k);
```

```
    CH3c(:,k)=H.*CH3(:,k);
    CH2fft(:,k) = fft(CH2c(:,k));
    P2CH2(:,k) = abs(CH2fft(:,k)/L);
    NP2CH2(:,k) = P2CH2(:,k);
    P1CH2(:,k) = NP2CH2(1:L/2+1,k);
    P1CH2(2:end-1,k) = 2*P1CH2(2:end-1,k);
    CH3fft(:,k) = fft(CH3c(:,k));
    P2CH3(:,k) = abs(CH3fft(:,k)/L);
    NP2CH3(:,k) = P2CH3(:,k);
    P1CH3(:,k) = NP2CH3(1:L/2+1,k);
    P1CH3(2:end-1,k) = 2*P1CH3(2:end-1,k);
end

% Compute FFT of Force

for k=1:70
    CH1c(:,k)=H.*CH1(:,k);
    CH1fft(:,k) = fft(CH1c(:,k));
    P2CH1(:,k) = abs(CH1fft(:,k)/L);
    NP2CH1(:,k) = P2CH1(:,k);
    P1CH1(:,k) = NP2CH1(1:L/2+1,k);
end

% Response FFT divided by Force FFT

for k=1:70
    CH2_CH1(:,k)=P1CH2(:,k)./P1CH1(:,k);
    CH3_CH1(:,k)=P1CH3(:,k)./P1CH1(:,k);
end

%T=Press_time(2)-Press_time(1);
%Fs=1/T;
Fs=12800;
f=Fs*(0:(L/2))/L;
```

B.5 Kurtosis Analysis

```
% Kurtosis Analysis for Acoustic Data
% (c) 2018 Jacob Davis

% I:index number total

% Std_dev: sigma(y) = sqrt((1/I)*sum((y_i-y_bar)^2))

% Absolute Kurtosis: AK(y) = (1/I)*sum((y_i-y_bar)^4)
```

```
% Normalized Kurtosis: NK(y) = AK(y)/((sigma(y)^2)^2)


clear
load FullCorrectedDataV2.mat

% For Time signal

I=1024;
for k=1:70
    CH2_mean(1,k)=mean(CH2(:,k));
    CH3_mean(1,k)=mean(CH3(:,k));
end
for k=1:70
    for j=1:1024
        s2(j,k) = CH2(j,k)-CH2_mean(1,k);
        s3(j,k) = CH3(j,k)-CH3_mean(1,k);
        ss2(j,k) =s2(j,k)^4;
        ss3(j,k) =s3(j,k)^4;
    end
    AK_time_CH2(1,k) = (1/I)*sum(ss2(:,k));
    AK_time_CH3(1,k) = (1/I)*sum(ss3(:,k));
end

save KurtosisTimeData.mat
T=table(datalabel(:,1:3),AK_time_CH2',AK_time_CH3');
writetable(T,'Kurtosis_Time.xlsx','sheet',1)

%AK(y) = (1/I)*sum((y_i-y_bar)^4)

clear
load FFTData.mat
I=513;

for k=1:70
    CH2fftmean(1,k) = mean(CH2_CH1(:,k));
    CH3fftmean(1,k) = mean(CH3_CH1(:,k));
    for j=1:513
        fft_s2(j,k) = CH2_CH1(j,k)-CH2fftmean(1,k);
        fft_s3(j,k) = CH3_CH1(j,k)-CH3fftmean(1,k);
        fft_ss2(j,k) = fft_s2(j,k)^4;
        fft_ss3(j,k) = fft_s3(j,k)^4;
    end
    AK_fft_CH2(1,k) = (1/I)*sum(fft_ss2(:,k));
    AK_fft_CH3(1,k) = (1/I)*sum(fft_ss3(:,k));
```

```
end

save KurtosisFFTData.mat
Q=table(datalabel(:,1:3),AK_fft_CH2',AK_fft_CH3');
writetable(Q,'Kurtosis_FFT.xlsx','sheet',1)
```